Internet Appendix for:

Common shocks in stocks and bonds

Anna Cieslak and Hao Pang*

This version: October 2020

(Not intended for publication)

*Anna Cieslak (corresponding author): Duke University, Fuqua School of Business, NBER, and CEPR, e-mail: anna.cieslak@duke.edu. Hao Pang: Duke University, Fuqua School of Business, e-mail: hao.pang@duke.edu.

A. Summary of identification restrictions

This appendix summarizes our identification restrictions. We impose the following restrictions, all on the contemporaneous impact of ω_t shocks on innovations in asset prices: (i) *sign restrictions* that determine the direction in which a shock moves yields and stocks; (ii) *between-asset restrictions* that determine the relative effect of shock ω^i on different elements of Y; and (iii) *within-asset restrictions* that determine the relative importance of different shocks for a given element Y^j.

Using the $+/-$ signs to denote the direction of an impact of a positive shock ($\omega^i > 0$), we assume that

$$\tilde{A} = \begin{pmatrix} A_g^{(2)} & A_m^{(2)} & A_{p+}^{(2)} & A_{p-}^{(2)} \\ A_g^{(5)} & A_m^{(5)} & A_{p+}^{(5)} & A_{p-}^{(5)} \\ A_g^{(10)} & A_m^{(10)} & A_{p+}^{(10)} & A_{p-}^{(10)} \\ A_g^{s} & A_m^{s} & A_{p+}^{s} & A_{p-}^{s} \end{pmatrix} \begin{pmatrix} \sigma_g & 0 & 0 & 0 \\ 0 & \sigma_m & 0 & 0 \\ 0 & 0 & \sigma_{p+} & 0 \\ 0 & 0 & 0 & \sigma_{p-} \end{pmatrix} = \begin{pmatrix} + & + & - & + \\ + & + & - & + \\ + & + & - & + \\ + & - & - & - \end{pmatrix}. \tag{IA.23}$$

Superscripts (2), (5), and (10) refer to yield maturity, superscript s refers to the stock market response, and subscripts label the shocks. Growth ω^g and the hedging premium ω^{p+} shocks move stocks and yields in the same direction (first and third column of $\tilde{A}$), whereas monetary ω^m and common premium ω^{p-} shocks move stocks and yields in opposite directions (second and fourth column of $\tilde{A}$). It is clear that sign restrictions themselves do not allow to distinguish ω^g from ω^{p+} and ω^m from ω^{p-}. This separation is achieved by imposing additional conditions on how shocks propagate along the maturity dimension of the yield curve.

The between-asset restrictions involve yields at different maturities and are imposed on elements of a column j of $\tilde{A}$, $\tilde{A}(:,j)$. Given that σ's are all strictly positive, imposing between-asset restrictions on $\tilde{A}$ is equivalent to imposing them on A. Growth and monetary shocks, ω^g and ω^m, drive the short end of the yield curve more than the long end of the yield curve, while the opposite holds for the risk-premium shocks, ω^{p+} and ω^{p-}. For the monetary shock, we have $A_m^{(2)} > A_m^{(5)} > A_m^{(10)}$. For the risk-premium shocks, we flip the inequality sign. For growth shocks, we require that $A_g^{(2)} > A_g^{(10)}$ and $A_g^{(5)} > A_g^{(10)}$, but we do not constrain the relationship between $A_g^{(2)}$ and $A_g^{(5)}$ based on the evidence that growth news can exert a non-monotonic effect at short and intermediate maturities.

The within-asset restrictions constrain the relative contributions of different shocks to conditional volatilities of yields. These are constraints on the elements of a given row i of $\tilde{A}$, $\tilde{A}(i,:)$. Specifically, we assume that the conditional variance of the ten-year yield is to a larger extent determined by the risk-premium shocks than it is by shocks to short-rate expectations—growth and monetary shocks—and conversely for the two-year yield, i.e., $\frac{(A_m^{(2)}\sigma_m)^2+(A_g^{(2)}\sigma_g)^2}{(A_{p^+}^{(2)}\sigma_{p^+})^2+(A_{p^-}^{(2)}\sigma_{p^-})^2} > 1$ for the two year yield and $\frac{(A_m^{(10)}\sigma_m)^2+(A_g^{(10)}\sigma_g)^2}{(A_{p^+}^{(10)}\sigma_{p^+})^2+(A_{p^-}^{(10)}\sigma_{p^-})^2} < 1$ for the ten-year yield. Those restrictions are consistent with the evidence on the properties of interest rate volatility (e.g., Cieslak and Povala, 2016).

A concise list of all restrictions is below.

Sign restrictions:

We impose 16 sign restrictions on each of the 16 entries of A.

$$\begin{pmatrix} A_g^{(2)} > 0 & A_m^{(2)} > 0 & A_{p+}^{(2)} \leq 0 & A_{p-}^{(2)} > 0 \\ A_g^{(5)} > 0 & A_m^{(5)} > 0 & A_{p+}^{(5)} \leq 0 & A_{p-}^{(5)} > 0 \\ A_g^{(10)} > 0 & A_m^{(10)} > 0 & A_{p+}^{(10)} \leq 0 & A_{p-}^{(10)} > 0 \\ A_g^{s} > 0 & A_m^{s} \leq 0 & A_{p+}^{s} \leq 0 & A_{p-}^{s} \leq 0 \end{pmatrix} \tag{IA.24}$$

Between-asset restrictions:

Growth shock: $|A_g^{(2)}| > |A_g^{(10)}|$ and $|A_g^{(5)}| > |A_g^{(10)}|$,
Monetary policy shock: $|A_m^{(2)}| > |A_m^{(5)}| > |A_m^{(10)}|$,

Hedging risk premium shock: $|A^{(2)}_{p+}| < |A^{(5)}_{p+}| < |A^{(10)}_{p+}|$,
Common risk premium shock: $|A^{(2)}_{p-}| < |A^{(5)}_{p-}| < |A^{(10)}_{p-}|$.

Within-asset restrictions:

Two-year yield: $(A^{(2)}_m\sigma_m)^2 + (A^{(2)}_g\sigma_g)^2 > (A^{(2)}_{p+}\sigma_{p+})^2 + (A^{(2)}_{p-}\sigma_{p-})^2$
Ten-year yield: $(A^{(10)}_m\sigma_m)^2 + (A^{(10)}_g\sigma_g)^2 < (A^{(10)}_{p+}\sigma_{p+})^2 + (A^{(10)}_{p-}\sigma_{p-})^2$

B. Stability of the structural relations and time-varying volatility

This appendix discusses the implications of time-varying volatility of structural shocks for our identification. Figure IA-7 presents shocks estimated over the 1983–2017 versus different subsamples, showing that they are highly correlated. The goal of this appendix is to provide additional interpretation of these results.

Suppose that the true structural model is

$$Y_{t+1} = \mu + \Psi Y_t + A\Sigma_t\omega_{t+1}, \tag{IA.25}$$

where A is the true contemporaneous structural response matrix, Σ_t is the conditional volatility of structural shocks at time t (diagonal matrix with σ^i_t on the diagonal), and ω_t are iid shocks with $Var(\omega_t) = I$. The reduced-form innovations in asset prices are $u_t = A\Sigma_t\omega_t$. We want to assess the effect of applying our identification that assumes constant volatility, when the true model is (IA.25). Intuitively, the shocks we recover (denoted $\tilde{\omega}_t$ below) are not iid but have time-varying volatility.

For illustration, we consider a simple example with two regimes for Σ_t, but the intuition extends to more general dynamics of Σ_t. Assume the full sample has N observations, with $\Sigma_t = \Sigma_1$ for the first N_1 observation (subsample 1, $t \in \{1, ..., N_1\}$), and $\Sigma_t = \Sigma_2$ for the next N_2 observations (subsample 2, $t \in \{N_1 + 1, ..., N\}$), where $N_1 + N_2 = N$. We observe the reduced-form innovations in asset prices u_t. If we know the true value of $A\Sigma_t$, we can back out the structural shocks as $\omega_t = (A\Sigma_t)^{-1}u_t$. With two volatility regimes, $\omega_t = (A\Sigma_1)^{-1}u_t$ for $1 \le t \le N_1$ and $\omega_t = (A\Sigma_2)^{-1}u_t$ for $N_1 + 1 \le t \le N$.

Let us now consider what happens if we recover shocks using a constant covariance matrix of reduced-form innovations u_t calculated over the full sample. The reduced-form covariance matrix of innovations in subsample i is $\Omega_i = A\Sigma_i\Sigma_i'A'$, $i \in \{1, 2\}$. Thus, the variance-covariance matrix of reduced-form shocks computed over the full sample is $\Omega = \frac{N_1}{N}\Omega_1 + \frac{N_2}{N}\Omega_2 = A(\frac{N_1}{N}\Sigma_1\Sigma_1' + \frac{N_2}{N}\Sigma_2\Sigma_2')A'$ and we define

$$\Sigma\Sigma' = \frac{N_1}{N}\Sigma_1\Sigma_1' + \frac{N_2}{N}\Sigma_2\Sigma_2'. \tag{IA.26}$$

$\Sigma\Sigma'$ can be viewed as the weighted average of the true conditional variances of structural shocks, with $\Omega = A\Sigma\Sigma'A'$. Thus, by imposing a constant conditional volatility, we recover $\tilde{\omega}_t = (A\Sigma)^{-1}u_t$ for $1 \le t \le N$ with sample variance of $\tilde{\omega}_t$ normalized to unity $\widehat{Var}(\tilde{\omega}_t) = I$. The relationship between $\tilde{\omega}_t$ shocks and the true ω_t is

$$\tilde{\omega}_t = \Sigma^{-1}\Sigma_1\omega_t \quad \text{for} \quad 1 \le t \le N_1, \tag{IA.27}$$
$$\tilde{\omega}_t = \Sigma^{-1}\Sigma_2\omega_t \quad \text{for} \quad N_1 + 1 \le t \le N. \tag{IA.28}$$

Let us also define

$$D_i = \Sigma^{-1}\Sigma_i,\ i = \{1, 2\} \tag{IA.29}$$

to be a diagonal scaling matrix and note that

$$\Omega_i = A\Sigma_i\Sigma_i'A' = A\Sigma D_i D_i'\Sigma'A'. \tag{IA.30}$$

This implies that in a given subsample, $\tilde{\omega}_t$ will not have a unit variance. For example, if the conditional volatility associated with s-th shock is higher in subsample 1 than in subsample 2 ($\sigma_1^s > \sigma_2^s$), then $\tilde{\omega}_t^s = \frac{\sigma_1^s}{\sigma^s}\omega_t^s$ for $1 \leq t \leq N_1$, $\frac{\sigma_1^s}{\sigma^s} > 1$, and hence the variance of $\tilde{\omega}_t^s$ will be above unity in subsample 1 and below unity in subsample 2. This is the intuition behind results in Figure IA-7, where the shocks estimated over subsample are close to but not exactly on the 45-degree line.[1]

The above analysis indicates that, under the assumption that matrix A is constant (i.e., structural relations in the economy do not change over time), we are able to recover structural shocks up to the scaling by their time-varying volatilities. As such, the historical decompositions of yield changes and stock returns in equation (10) will correctly describe the contributions of structural shocks given that $A\Sigma J_{ss}\tilde{\omega}_t = A\Sigma_i J_{ss}\omega_t$ for shocks indexed by s and a subsample $i = \{1, 2\}$.

One implication of the setting in equation (IA.25) is that the only way the covariance of stocks and yields can move around over time is due to time-varying volatilities of structural shocks. To understand if this is plausible empirically, we analyze if the constant A assumption is consistent with the switching sign of the stock-yield covariances we observe empirically. We treat the 1983–1997 period as subsample 1 and 1998–2017 period as subsample 2. In practice, we do not observe the true value of $A\Sigma_t$, but rather we use the median-target (MT) solution over the full 1983–2017 sample as point estimate of $\tilde{A} = A\Sigma$. Let us denote the full-sample MT solution as $\widehat{\tilde{A}}$. We estimate reduced-form variance-covariances of innovations from VAR(1) residuals over the two subsamples, $\widehat{\Omega}_1, \widehat{\Omega}_2$. Then, we search for empirical analogs of the diagonal scaling matrices $\widehat{D}_1$ and $\widehat{D}_2$ defined in equation (IA.29) by minimizing $\widehat{D}_i = \underset{D_i}{\text{argmin}}||\frac{\widehat{\Omega}_i - \widehat{\tilde{A}} D_i D_i' \widehat{\tilde{A}}'}{\widehat{\Omega}_i}||$, where $\widehat{D}_i$ is a diagonal matrix and where we keep $\widehat{\tilde{A}}$ constant at the full-sample value. The norm $||\cdot||$ is a 2-norm of matrix (approximately the maximum singular value of a matrix),[2] and the fraction denotes element-wise division, which serves to standardize the differences across elements of $\widehat{\Omega}_i$. Note that, if we replace all the hat terms with their true value, the norm should be equal to 0.

The difference between D_1 and D_2 describes how the volatility of structural shocks varies across the two subsamples. For 1983–1997 and 1998–2017 samples, respectively, we have

$$\widehat{D}_1 = \begin{pmatrix} 0.93 & 0 & 0 & 0 \\ 0 & 1.16 & 0 & 0 \\ 0 & 0 & 0.66 & 0 \\ 0 & 0 & 0 & 1.18 \end{pmatrix}, \quad \widehat{D}_2 = \begin{pmatrix} 1.05 & 0 & 0 & 0 \\ 0 & 0.84 & 0 & 0 \\ 0 & 0 & 1.17 & 0 \\ 0 & 0 & 0 & 0.81 \end{pmatrix}$$

where the diagonal elements are ordered to correspond to $\omega^g, \omega^m, \omega^{p+}, \omega^{p-}$ shocks. We can now compare the reduced-form covariances that are consistent with the constant A assumption (at the full-sample MT solution) with unconstrained equivalents $\widehat{\Omega}_i$ in each subsample i:

$$\widehat{\Omega}_1 = \begin{pmatrix} 0.004 & 0.004 & 0.003 & -0.012 \\ 0.004 & 0.004 & 0.004 & -0.019 \\ 0.003 & 0.004 & 0.004 & -0.022 \\ -0.012 & -0.019 & -0.022 & 0.894 \end{pmatrix}, \quad \widehat{\tilde{A}}\widehat{D}_1\widehat{D}_1\widehat{\tilde{A}}' = \begin{pmatrix} 0.003 & 0.003 & 0.003 & -0.012 \\ 0.003 & 0.004 & 0.004 & -0.016 \\ 0.003 & 0.004 & 0.004 & -0.021 \\ -0.012 & -0.016 & -0.021 & 1.103 \end{pmatrix}$$

$$\widehat{\Omega}_2 = \begin{pmatrix} 0.003 & 0.003 & 0.002 & 0.020 \\ 0.003 & 0.004 & 0.003 & 0.024 \\ 0.002 & 0.003 & 0.004 & 0.023 \\ 0.020 & 0.024 & 0.023 & 1.455 \end{pmatrix}, \quad \widehat{\tilde{A}}\widehat{D}_2\widehat{D}_2\widehat{\tilde{A}}' = \begin{pmatrix} 0.003 & 0.003 & 0.003 & 0.020 \\ 0.003 & 0.004 & 0.003 & 0.023 \\ 0.003 & 0.003 & 0.004 & 0.023 \\ 0.020 & 0.023 & 0.023 & 1.226 \end{pmatrix}$$

Recall that both ω^{p+} and ω^g (ω^m and ω^{p-}) shocks move yields and stocks in the same (opposite) direction. We see that the time-varying volatility of structural shocks alone can generate a switching sign of the stock-yield covariances. In particular, the switch from negative to positive stock-yield covariance in the late 1990s is due to the increase in volatility of the hedging premium shocks ω^{p+} and decrease in the volatility of the

[1] We note that regressions in Figure IA-7 do not impose that A is constant in subsamples and equal to the full sample estimates.

[2] The 2-norm of an $m \times m$ matrix M is defined by $\max_{\vec{v} \neq \vec{0}} \frac{||M\vec{v}||_2}{||\vec{v}||_2}$, where $\vec{v}$ is a non-zero m-dimensional vector.

common premium shocks ω^{p-}; this effect is amplified by the increased volatility of growth news ω^g and decline in volatility of monetary news ω^m.

C. Cross-maturity restrictions

C.1. Two-factor term structure example

To illustrate our restrictions across yield maturities, we consider a simple affine yield-curve model with two state variables: the short rate i_t and the price-of-risk (pure risk-premium) factor x_t. Each state variable follows an AR(1) process:

$$i_{t+1} = \mu_i + \phi_i i_t + \sigma_i \varepsilon^i_{t+1} \tag{IA.31}$$

$$x_{t+1} = \mu_x + \phi_x x_t + \sigma_x \varepsilon^x_{t+1}, \tag{IA.32}$$

where $\begin{pmatrix} \varepsilon^i_{t+1} \\ \varepsilon^x_{t+1} \end{pmatrix} \sim N(\mathbf{0}, I_{2\times 2})$. We assume that ε^i_{t+1} shocks are priced and investors require a time-varying risk premium for exposure to ε^i_{t+1} that varies with x_t. Thus, the log stochastic discount factor (SDF) has the form

$$\xi_{t+1} = \ln M_{t+1} = -i_t - \frac{1}{2}(\frac{\lambda_x}{\sigma_x})^2 x_t^2 - \frac{\lambda_x}{\sigma_x} x_t \varepsilon^i_{t+1}. \tag{IA.33}$$

In this setting, risk premia in yields for all maturities move only with x_t. The one-period yield is $y^{(1)}_t = i_t$. Using standard arguments, yields are affine in the state variables:

$$y^{(n)}_t = b_n + B^i_n i_t + B^x_n x_t, \tag{IA.34}$$

and shocks to yields are

$$y^{(n)}_{t+1} - E_t(y^{(n)}_{t+1}) = B^i_n \sigma_i \varepsilon^i_{t+1} + B^x_n \sigma_x \varepsilon^x_{t+1}. \tag{IA.35}$$

The effect of shocks to the state variables across yield maturities is determined by the B_n loadings, which solve the standard recursive equations (see also Appendix F):

$$B^i_n = \frac{1}{n}\frac{1-\phi_i^n}{1-\phi_i} \tag{IA.36}$$

$$B^x_n = \frac{n-1}{n}\phi_x B^x_{n-1} - \frac{n-1}{n} B^i_{n-1}\lambda_x \tag{IA.37}$$

$$= -\frac{\lambda_x}{n(1-\phi_i)} \sum_{j=1}^{n-1} (1-\phi_i^{n-j})\phi_x^{j-1} \tag{IA.38}$$

$$= -\frac{\lambda_x}{n(1-\phi_i)} (\frac{1-\phi_x^{n-1}}{1-\phi_x} - \sum_{j=1}^{n-1} \phi_i^{n-j}\phi_x^{j-1}) \tag{IA.39}$$

with initial conditions $B^i_1 = 1$ and $B^x_1 = 0$.

If $0 < \rho_i < 1$, the loadings of yields on i_t decline with maturity, $B^i_n - B^i_{n-1} < 0$, as a consequence of the mean reversion in i_t. Appendix C.2 extends this result to a multivariate case.

The effect of x_t across maturities is more complex because it depends on the persistence of both state variables. In general, the effect of risk premium shocks x_t on yields can be non-monotonic (hump-shaped) across maturities. However, we argue that for empirically meaningful levels of persistence of shocks to the short rate and the risk premia (ϕ_i and ϕ_x in the example above) and for the range of maturities we are interest in (up to ten years), the effect of risk-premium shocks increases with maturity. To inspect how the loadings on x_t change with maturity, consider

$$B_n^x - B_{n-1}^x = \underbrace{(\frac{n-1}{n}\phi_x - 1)B_{n-1}^x}_{\text{1st term}} \underbrace{-\frac{n-1}{n}B_{n-1}^i\lambda_x}_{\text{2nd term}}. \tag{IA.40}$$

Let us assume that $\lambda_x < 0$, so that $B_n^x > 0$.[3] The second term on the right-hand side of equation (IA.40) is positive and drives the increasing impact of the price-of-risk factor x_t with maturity. The strength of that increase is dictated by the persistence of the short rate i_t, which is the source of priced shocks in the yield curve. Intuitively, investors holding long-term bonds face more exposure to short-rate shocks if those shocks are more persistent (the higher ϕ_i). As such, the impact of the time-varying risk-premium x_t for bearing persistent exposure to short-rate shocks increases with yield maturity. However, the first term on the right-hand side of (IA.40) is negative, thus counteracting the second term. The first term becomes more negative the lower the persistence of the price-of-risk factor x_t: If the price of risk shocks are highly transitory, then their effect will start dying out as the maturity lengthens. Overall, the increasing effect of the risk-premium factor across maturities is more pronounced if shocks that are priced (short-rate shocks) as well as shocks that drive the risk premium are both relatively persistent.

As an illustration, Figure IA-1 displays B_n^x loadings as a function of maturity for different combinations of AR(1) coefficients ϕ_x and ϕ_i, which are expressed in annual terms. For reference, the thick black line in each graph indicates loadings obtained for parameters calibrated in the data: $\phi_i = 0.93$ and $\phi_x = 0.45$. Over the 1983–2017 sample, the AR(1) coefficient for the one-year Treasury yield is 0.994 at a monthly frequency, and hence $\phi_i = 0.93 (= (0.994)^{12})$ at an annual frequency. We calibrate the persistence of the risk-premium factor, $\phi_x = 0.45 (= (0.935)^{12})$, using the monthly estimates of the time-varying bond risk premium from Cieslak and Povala (2015).[4] For the graph, we assume $\lambda_x = -0.5$ (this parameter does not impact the monotonic pattern of loadings across maturities). The persistence parameters calibrated using the time-series data could be thought as providing a lower bound on the persistence actually perceived by investors, given the evidence on sluggish short-rate expectations updating in the literature (Brooks et al., 2019, Cieslak, 2018, e.g.,).

Figure IA-1 shows that the impact of the price-of-risk factor x_t generally increases steeply between maturities of two and five years and then flattens out. If short-rate shocks are relatively transitory, x_t can have a declining effect on yields starting from intermediate maturities. However, as we argue in the body of the paper, models estimated in the literature strongly suggest that the risk-premium effect increases for maturities up to at least ten years, which is consistent with our simple calibration and relatively persistent shocks to short-rate expectations. It is also worth noting that this result does not require an extreme persistence of the risk-premium itself.

C.2. Effect of short-rate shocks on long-term yields under the expectations hypothesis

In this appendix, we discuss how state variables driving the short rate affect longer maturity yields in a multivariate case. We consider a pure expectations hypothesis (EH) case. Under the EH, the long-term yield is the average of expected future short rates:

$$y_t^{(n),EH} = \frac{1}{n}E_t\left(\sum_{i=0}^{n-1} y_{t+i}^{(1)}\right). \tag{IA.41}$$

In affine dynamic term structure models, the short rate is $y_t^{(1)} = \gamma_0 + \gamma' X_t$, where X_t are the state variables. It is common to specify X_t as a VAR(1) process with a mean reversion matrix Φ (omitting constants for simplicity):

$$X_t = \Phi X_{t-1} + \epsilon_t. \tag{IA.42}$$

[3] This assumption is without loss of generality because λ_x does not change the monotonicity pattern of the B_n^x loadings (see equation (IA.39)).

[4] Alternatively, the Cochrane and Piazzesi (2005) factor implies an annual persistence of 0.43 over the same period.

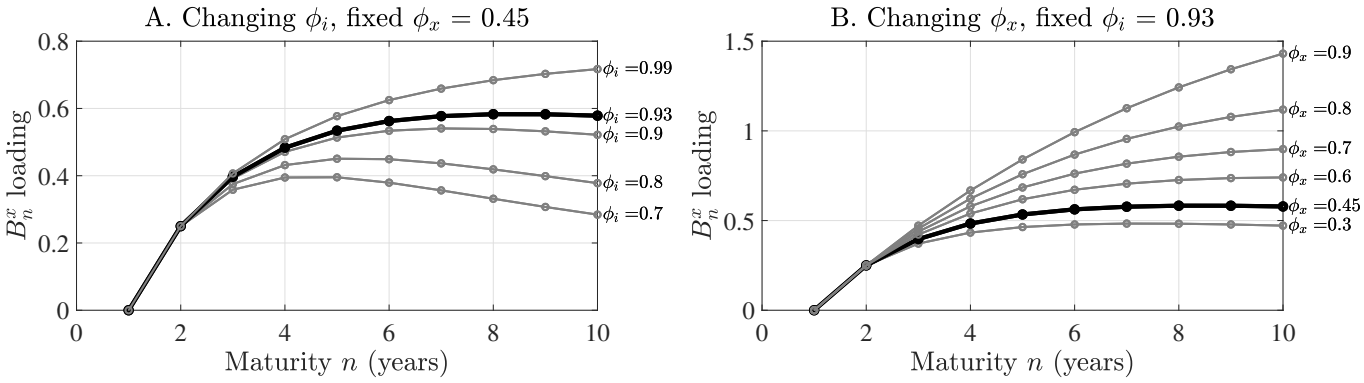

Figure IA-1. Example: B_n^x loadings in a simple two-factor affine model. The figure presents loadings of yields on the market-price-of-risk factor x_t in a two-factor affine model. Parameter ϕ_i and ϕ_x are expressed in annual terms. The thick black lines indicate loadings for persistence parameters calibrated in the data.

Then, under the EH, the long-term yield is

$$y_t^{(n),EH} = \text{const.} + \frac{1}{n}\gamma'(I-\Phi)^{-1}(I-\Phi^n)X_t. \tag{IA.43}$$

Suppose all eigenvalues of Φ are distinct,[5] then $\Phi = C\Lambda C^{-1}$, Λ is the diagonal matrix of eigenvalues with elements λ_i, $\lambda_j \neq \lambda_i$, C is the matrix of associated eigenvectors. Let $Z_t = C^{-1}X_t$, then

$$Z_t = \Lambda Z_{t-1} + C^{-1}\epsilon_t. \tag{IA.44}$$

The short rate is $y_t^{(1)} = \gamma' X_t = \gamma' C Z_t$, and the long-term rate is

$$y_t^{(n),EH} - \text{const.} = \gamma'(\frac{1}{n}(I-\Phi)^{-1}(I-\Phi^n))X_t = \gamma'(\frac{1}{n}\sum_{i=0}^{n-1}\Phi^i)X_t = \tag{IA.45}$$

$$\gamma'(\frac{1}{n}\sum_{i=0}^{n-1}C\Lambda^i C^{-1})CZ_t = \gamma' C(\frac{1}{n}\sum_{i=0}^{n-1}\Lambda^i)Z_t = \gamma' C\tilde{\Lambda}Z_t \tag{IA.46}$$

where $\tilde{\Lambda}$ is diagonal with element i given by $\tilde{\lambda}_i = \frac{1}{n}\frac{1-\lambda_i^n}{1-\lambda_i}$, $\tilde{\lambda}_i < 1$ if $\lambda_i < 1$. So as n increases the impact of the short rate shocks will be dampened as long as elements of $\tilde{\Lambda}$ are less then unity, $|\lambda_i| < 1$, analogous to the univariate AR(1) case.

D. Regressions of stock returns and yield changes on macroeconomic expectations survey updates

To further motivate the restrictions on growth shocks, we provide evidence based on updates of expectations about the real GDP (RGDP) growth from the Blue Chip Economic Indicators (BCEI) survey. The survey is available at a monthly frequency. Survey updates proxy for innovations in forecasters' beliefs about economic growth (e.g., Romer and Romer, 2004). While survey updates do not represent structural shocks in the sense of Section 2.1, they should be highly correlated with growth news we aim to identify.

[5] One can relax the assumption that all eigenvalues are distinct (thus Φ is not necessarily diagonalizable). The only assumption needed for this case is that all eigenvalues are less than unity in norm $|\lambda| < 1$. The proof is available upon request.

We define the forecast update at horizon h as the revision in forecasts between two consecutive surveys (in month $t-1$ and t) for the same future calendar quarter, $\text{Updt}_t(Z_h) = F_t(Z_h) - F_{t-1}(Z_h)$, where $F_t(Z_h)$ denotes forecast formed in month t, and h denotes forecast horizon (in quarters) relative the forecast month t (making sure that forecasts at t and $t-1$ refer to the same quarter). Given available data, we can construct updates from the current quarter ($h = 0q$) up to three quarters ahead ($h = 3q$). For example, an update observed in January 2000 (time t) for the current quarter ($h = 0q$), $\text{Updt}_t(g_0)$, is the change between the January 2000 and December 1999 survey forecast of what the real GDP growth rate will be in the first quarter of 2000.

In Table IA-1, we regress monthly S&P 500 index returns and zero-coupon yield changes over the 1983–2017 sample on contemporaneous real GDP growth forecast updates, controlling for simultaneous updates of CPI inflation forecasts. We use nominal zero-coupon yields from Gürkaynak et al. (2006) and returns on the S&P 500 index from WRDS. The sample covers the 1983–2017 period, also used to produce the main results in the paper.[6]

Since survey forecasts are available for different horizons, a question arises about which horizon is appropriate. In general, we find that the explanatory power of real GDP forecast updates for stock returns and yield changes is stronger at shorter horizons. Inflation forecast updates, instead, have more explanatory power at longer horizons for yields and are generally insignificant at any horizon for stocks. Thus, in regressions in Table IA-1, we use the next quarter horizon ($h = 1q$) for the real GDP growth forecast update and three quarters ahead horizon ($h = 3q$) for the CPI inflation forecast update. The horizon of the real GDP growth forecast update is chosen based on Bayesian information criterion (BIC) for the stock return regression, and the horizon of the CPI forecast is chosen based on the average BIC across yield maturities. The loadings of yields on the real GDP growth update have a similar monotonic pattern across maturities when we use the current quarter forecast (nowcast, $h = 0q$), and become generally insignificant at longer horizons.

Table IA-1 shows that for stock returns (column (1)) the coefficient on the real GDP update is positive, implying that a 1% per annum upward revision of growth expected next quarter is associated with 5.8% higher stock returns in a given month ($t = 3.6$). For yields, a 1% growth update raises the two-year yield (column (3)) by 25 bps ($t = 4$) and the ten-year yield by only 7 bps ($t = 1$), with the difference between the coefficients significant at the 1% level (column (8)). Hence, the declining effect of growth news across yield maturities is clearly visible. Expected inflation shocks do not have a significant contemporaneous effect on stocks, while their effect on the yield curve is flat across maturities, in line with the literature (Kozicki and Tinsley (2001), Rudebusch and Wu (2008), Cieslak and Povala (2015)).

	(1) Δs_t	(2) $\Delta y_t^{(1)}$	(3) $\Delta y_t^{(2)}$	(4) $\Delta y_t^{(3)}$	(5) $\Delta y_t^{(5)}$	(6) $\Delta y_t^{(7)}$	(7) $\Delta y_t^{(10)}$	(8) $\Delta(y^{(2)} - y^{(10)})$
RGDP updt $h = 1q$	5.81***	0.25***	0.24***	0.22***	0.18***	0.13**	0.072	0.17***
	(3.61)	(3.94)	(3.99)	(3.83)	(2.96)	(1.97)	(1.02)	(2.82)
CPI updt $h = 3q$	0.084	0.59***	0.66***	0.66***	0.64***	0.62***	0.58***	0.073
	(0.03)	(2.99)	(3.29)	(3.31)	(3.21)	(3.09)	(2.94)	(0.64)
R^2	0.12	0.12	0.11	0.094	0.073	0.057	0.044	0.062
N	420	420	420	420	420	420	420	420

Table IA-1. Effects of macroeconomic expectations updates on stock market returns and yield changes. The table presents regressions of monthly stock returns (column(1)) and yield changes (columns (2)–(7)) on updates to private sector expectations of real GDP growth and CPI inflation. Updates are in annualized percentage points. Column (8) tests the difference between the coefficients in columns (3) and (7), by regressing the changes in the spread between the two- and ten-year yield on the expectations updates. The horizon for the forecast updates is chosen based on Bayesian information criterion as described in the text. Dependent and explanatory variables are in percentages. Regressions are estimated with a constant, which is not displayed in the table. The sample period is 1983–2017. Robust t-statistics are reported in parentheses. $^{***}/^{**}/^{*}$ denotes significance at 1%/5%/10% level.

[6] Section 3.1 describes our data sources in more detail.

E. Link between ω shocks, inflation expectations, and nominal-real yield spread

In this section, we provide additional analysis of the link between the identified ω shocks, expected inflation, and the spread between nominal and real yields. We draw on evidence from survey expectations of inflation, TIPS, and inflation swaps.

E.1. Conceptual framework

To fix notation, we denote nominal yields with $y_t^{(n)}$ and real yields with $y_t^{(n),r}$:

$$y_t^{(n)} = \frac{1}{n}\sum_{i=0}^{n-1} E_t(y_{t+i}^{(1)}) + \psi_t^{(n)}, \tag{IA.47}$$

$$y_t^{(n),r} = \frac{1}{n}\sum_{i=0}^{n-1} E_t(y_{t+i}^{(1),r}) + \psi_t^{(n),r}, \tag{IA.48}$$

where $\psi_t^{(n)}$ and $\psi_t^{(n),r}$ denote the nominal and real term premium, respectively. The spread between nominal and real yields, the breakeven inflation rate (BEI), is

$$b_t^{(n)} = y_t^{(n)} - y_t^{(n),r} = \frac{1}{n}\sum_{i=1}^{n} E_t(\pi_{t+i}) + (\psi_t^{(n)} - \psi_t^{(n),r}). \tag{IA.49}$$

The first term on the right hand side of (IA.49) is the average expected inflation over the life of the bond, and the second term is the difference in risk premium between nominal and real yields. To clarify how equation (IA.49) relates to the shocks we identify, two points are worth highlighting.

First, $b_t^{(n)}$ spread (IA.49) can reflect both real and nominal factors, depending on the cyclical properties of inflation. In a model that allows growth expectations to feedback onto expected inflation (e.g., higher growth predicts higher inflation as when the economy is driven by demand shocks), both real and nominal shocks to the state variables will be reflected in the $b_t^{(n)}$ spread. In the illustrative model presented in Appendix F.4, if expected growth impacts expected inflation positively ($\phi_{\tau g} > 0$), then the spread $b_t^{(n)}$ will increase upon growth news and decline upon hedging premium news. Specifically, $\frac{\partial b_t^{(n)}}{\partial \omega^g} > 0$ due to the procylical expected inflation channel and $\frac{\partial b_t^{(n)}}{\partial \omega^{p+}} < 0$ due to the risk premium channel. The latter sign arises because, with procylical inflation, nominal bonds are even better hedges of growth risks than are real bonds.

Second, an important consideration is that exogenous expected inflation shocks could confound our empirical identification of monetary news. In Section 6.3 of the paper, we discuss conditions under which such situation can occur (see also Appendix F for extensions of the model presented in the paper). The basic intuition is that, with the Taylor principle satisfied (as is realistically the case over the sample we study), both expected inflation shocks and monetary shocks generate the same directional responses of stocks and nominal yields, and both have a diminishing effect across yield maturities. By studying how BEI rates respond to ω shocks, we can assess how large such confounding effects are. This is because, under realistic parameter configuration discussed in Appendix F.4, BEI should responds negatively to monetary news $\frac{\partial b_t^{(n)}}{\partial \omega^m} < 0$ (if monetary tightening leads to a downgrade of growth expectations) and positively to expected inflation news, $\frac{\partial b_t^{(n)}}{\partial \omega^\tau} > 0$. Below, we assess whether this is empirically the case.

E.2. Empirical analysis

To cast light on how ω shocks in our decomposition are related to expected inflation and BEI rates, we use TIPS, inflation swap rates, as well as survey expectations of inflation.

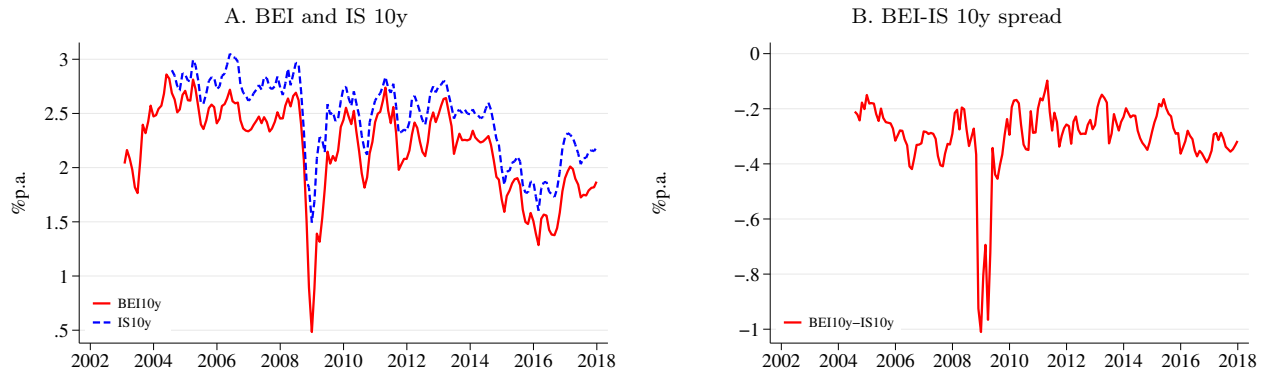

Figure IA-2. BEI and inflation swap rates. The figure uses within month averaged values of daily 10-year breakeven inflation rates (BEI) and inflation swap rates (IS).

One complication in using TIPS yields is that they contain an illiquidity premium relative to nominal Treasuries:

$$y_t^{(n),TIPS} = y_t^{(n),r} + L_t^{(n)}, \tag{IA.50}$$

$$BEI_t^{(n)} = y_t^{(n)} - y_t^{(n),TIPS} = b_t^{(n)} - L_t^{(n)}. \tag{IA.51}$$

$L_t^{(n)}$ captures the illiquidity of TIPS yields relative to nominal Treasury yields. The $L_t^{(n)}$ component could be correlated with the hedging (flight-to-safety) premium, in addition to any effect of the hedging premium present in the $b_t^{(n)}$ spread (via the procyclical inflation channel). As a proxy for illiquidity $L_t^{(n)}$, we therefore use the spread between BEI and inflation swap rates for the corresponding maturity, $L_t^{(n)} \approx BEI_t^{(n)} - IS_t^{(n)}$, where $IS_t^{(n)}$ is the rate on the zero-coupon inflation swap with maturity n. The BEI-IS spread should mainly capture the TIPS liquidity premium as the inflation swap market is relatively liquid (Andreasen et al., 2018, Fleckenstein et al., 2014, Pflueger and Viceira, 2016). BEI rates are available starting from January 2003[7] and IS rates from July 2004.

We first summarize empirical properties of inflation expectations and BEI rates, showing that the variation in BEIs is to a large degree driven by factors other than expected inflation news. We then link these quantities to the identified ω shocks.

E.2.1. Empirical properties of BEI rates and expected inflation

Figure IA-2 presents the time series of 10-year BEI and IS rates (Panel A) and their spread (Panel B) as a proxy for liquidity premium in TIPS, $L_t^{(n)}$. As reported by Fleckenstein et al. (2014), the BEI-IS spread can be large and widens during the global financial crisis.

Several facts are worth highlighting:

1. *BEI and IS rate changes are strongly positively correlated with stock returns.*
   Table IA-2 reports regressions of daily changes in BEI rates, IS rates, and BEI-IS spreads on contemporaneous daily stock returns. The strong positive relationship is present over the entire sample and when we exclude the global financial crisis (from July 2008 through May 2009), for both BEI and IS rates. Using BEI-IS spreads as a proxy for L_t, columns (5) and (6) show that the stock market

[7] We construct the BEI rates from GSW zero-coupon nominal and TIPS yield datasets. TIPS zero-coupon yields are available from 1999. However, extensive literature, including GSW, documents significant liquidity issues before 2003. The yield curve construction before 2003 relies on a limited number of bonds.

Panel A. All years

	(1) ΔBEI5y	(2) ΔBEI10y	(3) ΔIS5y	(4) ΔIS10y	(5) ΔBEI-IS5y	(6) ΔBEI-IS10y
Δs_t	0.288***	0.311***	0.250***	0.218***	-0.017	0.013
	(10.19)	(9.12)	(6.33)	(7.59)	(-0.43)	(0.53)
R^2	0.083	0.097	0.062	0.048	0.00028	0.00018
N (days)	3783	3783	3393	3393	3393	3393

Panel B. Excluding GFC

	(1) ΔBEI5y	(2) ΔBEI10y	(3) ΔIS5y	(4) ΔIS10y	(5) ΔBEI-IS5y	(6) ΔBEI-IS10y
Δs_t	0.289***	0.333***	0.269***	0.303***	-0.021	0.028
	(9.45)	(10.23)	(9.06)	(9.69)	(-0.90)	(1.37)
R^2	0.084	0.11	0.072	0.092	0.00042	0.00076
N (days)	3553	3553	3163	3163	3163	3163

Table IA-2. Regressions of daily changes in BEI and inflation swap rates on daily stock returns. The table presents regressions of daily BEI and IS rate changes for maturities of 5 and 10 years on contemporaneous stock returns. The last two columns report results for the changes in the spread between BEI and IS changes as a proxy for relative illiquidity of TIPS. BEI rates are available from January 2003 and IS rates from July 2004, both ending in December 2017. Panel B excludes the volatile period of the global financial crisis (GFC) from July 2008 through May 2009. Regression coefficients are standardized. HAC t-statistics with 22 daily lags are reported in parentheses to account for persistence in BEI residuals.

loadings on BEI are not different from those for IS. This suggests that the comovement between the stock returns and BEI changes is not driven by the relative illiquidity of TIPS. Below, we provide evidence that the comovement is consistent with the procyclical inflation mechanism highlighted in Section E.1.

2. *Expected real growth has explanatory power for the BEI.*
Table IA-3 presents regressions of changes in 5- and 10-year BEI on updates in inflation and real growth expectations from the Blue Chip Economic Indicators (BCEI) survey. We use updates for three quarters ahead because this is the longest horizon for which we can obtain consistent monthly time series for the post-2003 sample over which BEIs are available.[8] The regressions indicate that changes in BEI are positively related with updates to real growth expectations when controlling for inflation expectations updates, and the result holds when we exclude the financial crisis years. Including inflation updates in the regressions allows us to control for other determinants of expected inflation than growth. The positive loading of BEI on the growth update is consistent with procyclicality of inflation in the post-2003 period.

3. *Most of the variance in BEI rates comes from factors other than expected inflation.*
Figure IA-3, Panel A, show the dynamics of survey inflation forecasts at different horizons (current quarter, one, three, and four quarters ahead, and 10 years ahead). The median forecast of the 10-year-ahead annual average inflation is from the Survey of Professional Forecasters (SPF). The shorter-horizon forecasts are from the Blue Chip Economic Indicators (BCEI) survey. The graph shows that very short-term inflation expectations are highly volatile (which is primarily due to the food and energy prices), but the volatility declines rapidly with the forecast horizon. Forecasts at four quarters ahead and ten years ahead are nearly overlapping indicating that the term structure of expected inflation is approximately flat at horizons beyond a very short range. Figure IA-3 Panel B superimposes the

[8] As we show in Figure IA-3 Panel A, beyond very short forecast horizons, the term structure of expected inflation is flat, and thus the three-quarter ahead forecast should be highly correlated with long-term expected inflation embedded in the 5- and 10-year BEI.

	A. All years		B. Excl. GFC	
	(1) ΔBEI5y	(2) ΔBEI10y	(3) ΔBEI5y	(4) ΔBEI10y
$\text{Updt}_t(\Delta\text{CPI}_3)$	0.034	0.027	0.130*	0.174**
	(0.25)	(0.19)	(1.78)	(2.42)
$\text{Updt}_t(\Delta\text{RGDP}_3)$	0.505***	0.380***	0.299***	0.281***
	(2.79)	(4.24)	(4.28)	(3.99)
R^2	0.26	0.15	0.11	0.11
N (months)	179	179	168	168

Table IA-3. Regressions of BEI rate changes on inflation and real GDP growth updates. The table reports regressions of monthly changes in BEI rates on updates in inflation and real GRP forecasts in the BCEI survey. Panel A covers the 2003–2017 sample, panel B excludes the GFC period from July 2008 through May 2009. Regression coefficients are standardized. Robust t-statistics are in parentheses (using HAC t-statistics does not materially change the results).

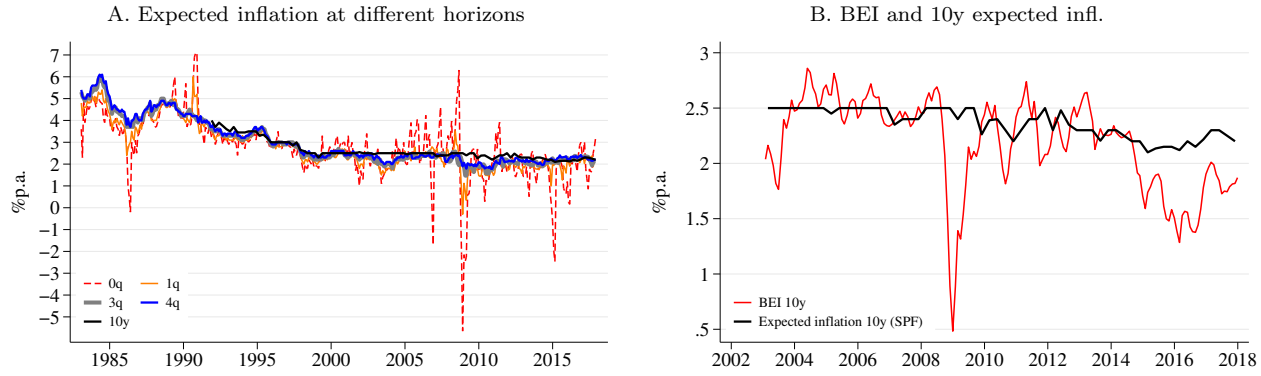

Figure IA-3. Expected inflation and BEI. Panel A plots survey forecasts of inflation at different horizons. Forecasts up to four quarters ahead (4q) are from the BCEI survey. They are annualized percent changes in CPI from the previous quarter. The long term forecast is from the Survey of Professional Forecasters (SPF), which is the forecast of the average inflation over the next 10 years. Panel B superimposes the SPF forecast against the 10-year BEI rate.

dynamics of inflation expectations with the 10-year BEI: inflation expectations account for a relatively small portion of the overall BEI variance. This suggests that most of the variance in BEI stems from the risk premium component.

E.2.2. Linking BEI changes to ω shocks

We now turn to connecting the variation in BEI rates to ω shocks. We study whether the signs of the loadings are consistent with the intuition we lay out in Section E.1, in particular with the procylical expected inflation channel. The predictions of how BEI rates should load on identified ω shocks are discussed in the model illustration in Appendix F.4.

In Table IA-4, we regress changes in the 5- and 10-year BEI rates on the identified shocks. We perform the analysis using all days (Panel A), all days excluding the financial crisis (Panel B), as well as only scheduled FOMC days (Panel C).

Focusing on Panels A and B of Table IA-4, the positive loadings of BEI changes on growth news aligns with the procyclical inflation expectations whereby higher expected growth leads to higher expected inflation.

These estimates support the results in Figure 7 Panel B of the paper showing that forecasters revise inflation expectations upward with growth news ω^g.

The estimates also confirm that variation in BEI is significantly related to the risk premium shocks (as suggested by Figure IA-3 Panel B). The negative sign of loadings on the hedging premium shocks ω^{p+} arises when procyclical inflation channel makes nominal bonds even more valuable in terms of hedging real growth risk than real bonds. The positive loading on the common premium shock ω^{p-} indicates that nominal bonds are more exposed than real bonds to variation to the nominal risk premium (as is the case when common premium drives compensation for both expected inflation shocks and monetary shocks). The economic significance of the common premium shocks, however, is about half of that of the hedging premium, in line with the increased importance of the hedging premium in recent decades.

Relative to other shocks, monetary shocks ω^m are least significant both in statistical and economic terms. Of note is the positive sign of the loadings. Appendix F.4 shows that BEI should be negatively exposed to monetary shocks if monetary policy tightening leads to lower growth expectations. We have argued that such a feedback effect is likely to be weak over our sample (e.g., Bauer and Swanson (2020)). The positive sign of the loadings in Table IA-4 could instead indicate that the identified ω^m shocks combine true monetary shocks with exogenous expected inflation shocks, a possibility we entertain in Section E.1. However, given that the positive estimate is marginally significant and much smaller than in case of other shocks, such confounding effect is unlikely to dominate our identification. The coefficient is to a large extent driven by the financial crisis period. In particular, during the financial crisis, the Fed's aggressive interest rate cuts coincided with falling inflation, thus inducing a positive comovement of BEI and monetary news in that episode.

The loadings of BEI changes on ω shocks also help clarify the sources of the strong positive comovement between BEI changes and stock returns in Table IA-2. Our decomposition attributes the positive comovement to the hedging premium shocks ω^{p+} (given that a positive ω^{p+} shock lowers both stock returns and BEIs). This result is related to Pflueger and Rinaldi (2020) who highlight the role of risk premium in generating the positive relationship between stock returns and BEI changes on FOMC days. To connect their finding to our decomposition more directly, in Panel C of Table IA-4, we regress changes in BEI rates on our identified shocks using only scheduled FOMC days. The hedging premium news ω^{p+} is the only significant shock for BEI changes on FOMC days.

The regressions of BEIs on identified shocks also agree with the findings of Hanson and Stein (2015) and Nakamura and Steinsson (2018) that BEI rates do not respond in a significant way to narrow-window monetary policy surprises. To summarize the results in this literature, Panel D of Table IA-4 shows that BEI changes are not significantly related to either target or path surprises identified by GSS/Swanson. From Table 2 in the paper, we know, in turn, that neither target nor path shocks are significantly related to the hedging premium news.[9] As such, the significance of hedging premium news in Panel C does not contradict the results in the earlier literature.

In summary, the results based on BEI regressions provide further support for the analysis in Section 6.1 of the paper that tie identified shocks to survey expectations of inflation and real GDP growth. The positive loading of BEI changes on growth news ω^g and the negative loading on the hedging premium news ω^{p+} are consistent with procyclical inflation during a large part of the sample period we analyze. The results also suggest that any potential confounding effect of exogenous expected inflation news is unlikely to significantly affect our identification (and economic interpretation) of ω shocks.

[9] In Table 2 in the main text, we show that target surprise is related to monetary news, while path shocks are a linear combination of monetary, growth and common premium news, but are not significantly related to the hedging premium news.

All days				
	A. All years		B. Excl. GFC	
	(1) ΔBEI5y	(2) ΔBEI10y	(3) ΔBEI5y	(4) ΔBEI10y
ω^g	0.285***	0.151***	0.269***	0.148***
	(9.99)	(6.18)	(10.74)	(6.52)
ω^m	0.073***	0.056**	0.048**	0.027
	(2.60)	(1.98)	(2.23)	(1.38)
ω^{p+}	-0.268***	-0.444***	-0.289***	-0.446***
	(-8.34)	(-14.40)	(-11.12)	(-17.36)
ω^{p-}	0.125***	0.237***	0.176***	0.278***
	(3.63)	(7.85)	(7.28)	(11.83)
R^2	0.19	0.30	0.23	0.35
N (days)	3783	3783	3553	3553
Scheduled FOMC days				
	C. Identified shocks		D. GSS shocks	
	(1) ΔBEI5y	(2) ΔBEI10y	(3) ΔBEI5y	(4) ΔBEI10y
ω^g	0.041	-0.065		
	(0.31)	(-0.46)		
ω^m	-0.081	-0.135		
	(-0.60)	(-1.17)		
ω^{p+}	-0.203**	-0.351***		
	(-2.01)	(-3.42)		
ω^{p-}	-0.185	0.004		
	(-1.26)	(0.03)		
Target			-0.189	-0.196
			(-1.00)	(-1.11)
Path			-0.060	-0.076
			(-0.56)	(-0.96)
R^2	0.077	0.18	0.042	0.048
N (days)	120	120	103	103

Table IA-4. Regressions of daily changes in BEI rates on daily ω shocks. Regression coefficients are standardized. The sample starts in 2003 when TIPS data becomes available. Panels A and B report HAC t-statistics (in parentheses) with 22 lags to account for any autocorrelation in the daily BEI residuals. Panels C and D report robust t-statistics.

F. Model illustration

This appendix provides the details on the affine model presented in Section 6.3. We discuss different parameter settings, how they affect the solutions, and what they imply for the identification restrictions we impose.

The factors follow a VAR(1) process:

$$F_{t+1} = \mu_F + \Phi_F F_t + \Sigma_F \omega_{t+1}, \tag{IA.52}$$

where $F_t = (\tau_t, g_t, m_t, x_t^+, x_t^-)'$, $\omega_{t+1} = (\omega_{t+1}^\tau, \omega_{t+1}^g, \omega_{t+1}^m, \omega_{t+1}^{x+}, \omega_{t+1}^{x-})'$. The nominal one-period interest rate is

$$i_t = \delta_0 + \delta_\tau \tau_t + \delta_g g_t + m_t = \delta_0 + \delta_1' F_t, \tag{IA.53}$$

where $\delta_1 = (\delta_\tau, \delta_g, 1, 0, 0)'$. The realized inflation is $\pi_{t+1} = \tau_t + \sigma_\pi \varepsilon_{t+1}^\pi$. The nominal log stochastic discount factor (SDF) has the form

$$\xi_{t+1} = \ln M_{t+1} = -i_t - \frac{1}{2}\Lambda_t'\Lambda_t - \Lambda_t'\omega_{t+1}, \tag{IA.54}$$

where $\Lambda_t = \Sigma_F^{-1}(\lambda_0 + \Lambda_1 F_t)$, which determines the time variation in risk premia. The real log SDF is $\xi_{t+1}^r = \xi_{t+1} + \pi_{t+1}$. We use superscript r to denote variables in real terms.

We first provide the general solution for yields, *pd* ratio and excess returns. We then consider different scenarios by imposing assumptions on Φ_F and Λ_1 matrices.

F.1. General solution for stocks and bonds

Nominal bonds. Letting $p_t^{(n)}$ denote the log price of an n-period nominal bond, and given nominal yields $y_t^{(n)} = -\frac{1}{n}p_t^{(n)}$, we conjecture that both yields and bond prices are affine in the state variables:

$$\begin{aligned} y_t^{(n)} &= b_n + B_n' F_t \\ p_t^{(n)} &= -n y_t^{(n)} = -n b_n - n B_n' F_t. \end{aligned} \tag{IA.55}$$

By no-arbitrage, nominal bond prices satisfy

$$\exp(p_t^{(n)}) = E_t[\exp(\xi_{t+1} + p_{t+1}^{(n-1)})]. \tag{IA.56}$$

We substitute the conjecture (IA.55) into the pricing equation (IA.56) and use the property of log-normal distribution to write out the expectation. As the pricing equation must hold for all values of the state variables, the nominal yield loadings on the state variables satisfy the following recursion:

$$B_n = \frac{n-1}{n}(\Phi_F - \Lambda_1)' B_{n-1} + \frac{1}{n}\delta_1. \tag{IA.57}$$

Because $y_t^{(1)} \equiv i_t$, where $i_t = \delta_0 + \delta_1' F_t$, we have the initial value $B_1 = \delta_1$ from which we iteratively obtain B_n for all $n \geq 2$.

The one-period expected log excess return on an n-period nominal bond is:

$$E_t(rx_{t+1}^{(n)}) + \frac{1}{2}Var_t(rx_{t+1}^{(n)}) = -Cov_t(\xi_{t+1}, p_{t+1}^{(n-1)} - p_t^{(n)}) = \text{const.} - (n-1)B_{n-1}'\Lambda_1 F_t. \tag{IA.58}$$

Real bonds. Letting $p_t^{(n),r}$ denote the log n-period real bond price. The real yield is $y_t^{(n),r} = -\frac{1}{n}p_t^{(n),r}$, which is also affine in the state variables:

$$y_t^{(n),r} = b_n^r + B_n^{r'} F_t \tag{IA.59}$$

with

$$B_n^r = \frac{(n-1)}{n}(\Phi_F - \Lambda_1)' B_{n-1}^r + \frac{1}{n}(\delta_1 - e_1), \tag{IA.60}$$

where e_1 is the first column of a 5×5 identity matrix. The initial value $B_1^r = \delta_1 - e_1 = (\delta_\tau - 1, \delta_g, 1, 0, 0)'$ is pinned down by the real short rate:

$$y_t^{(1),r} \equiv i_t^r = -\ln E_t[\exp(\xi_{t+1}^r)] = i_t - \tau_t - \frac{1}{2}\sigma_\pi^2 = \text{const.} + B_1^{r'} F_t. \tag{IA.61}$$

Stocks. Letting Δs_t denote the nominal log stock return, the Campbell-Shiller log-linearization implies

$$\Delta s_{t+1} = \kappa_0 + \kappa_1 pd_{t+1} + \Delta d_{t+1} - pd_t, \tag{IA.62}$$

where κ_0 and κ_1 are approximating constants determined only by the average *pd* ratio, with κ_1 slightly below 1. We assume the nominal realized dividend growth is $\Delta d_{t+1} = g_t + \sigma_d \varepsilon_{t+1}^d + \pi_{t+1}$. Stock returns in real terms are

$$\Delta s^r_{t+1} = \Delta s_{t+1} - \pi_{t+1}. \tag{IA.63}$$

We conjecture that the log *pd* ratio is affine in the state variables:

$$pd_t = b_s + B_s' F_t. \tag{IA.64}$$

Clearly, *pd* ratio is the same in nominal and real terms. By no-arbitrage, stock returns satisfy:

$$\ln E_t[\exp(\xi_{t+1} + \Delta s_{t+1})] = 0 \tag{IA.65}$$

Combining equation (IA.62), (IA.64), and (IA.65), we obtain the solution for the *pd* loadings on the state:

$$B_s' = (\delta_1' - \theta')[\kappa_1(\Phi_F - \Lambda_1) - I]^{-1}, \tag{IA.66}$$

where $\theta = (1, 1, 0, 0, 0)'$, and I is a 5×5 identity matrix. Plugging this result back into equation (IA.62), we have:

$$\Delta s_{t+1} = \text{const.} + (\kappa_1 B_s' \Phi_F - B_s' + \theta')F_t + \kappa_1 B_s' \Sigma_F \omega_{t+1} + \sigma_\pi \varepsilon^\pi_{t+1} + \sigma_d \varepsilon^d_{t+1} \tag{IA.67}$$

where $\tilde{\theta} = (0, 1, 0, 0, 0)'$. The responses to structural shocks ω are the same for nominal and real stock returns, and determined by $\kappa_1 B_s' \Sigma_F$. Therefore, we do not differentiate between the effect of ω shocks on nominal and real stock returns in the following discussion.

The one-period expected log excess nominal stock return is:

$$E_t(rx^s_{t+1}) + \frac{1}{2} Var_t(rx^s_{t+1}) = -Cov_t(\xi_{t+1}, \Delta s_{t+1}) = \text{const.} + \kappa_1 B_s' \Lambda_1 F_t. \tag{IA.68}$$

Expected log excess stock returns expressed in nominal and real terms differ only by a constant (as $-Cov(\xi^r_{t+1}, \Delta s^r_{t+1}) = -Cov(\xi_{t+1}, \Delta s_{t+1}) + \sigma^2_\pi$). Thus, the effect of ω shocks on the equity risk premium is $\kappa_1 B_s' \Lambda_1 \Sigma_F \omega_t$.

F.2. Baseline specification

Table IA-5 summarizes the baseline specification and the solutions we use in Section 6.3 to justify the sign restrictions in the empirical analysis. The specification in equation (20) of the paper implies that the SDF loadings matrix Λ_1 (equation (IA.54)) has two non-zero elements $\Lambda_{1(2,4)} = \lambda_{gx^+}$ and $\Lambda_{1(3,5)} = \lambda_{mx^-}$. In practice, we identify the signs of λ_{gx^+} and λ_{mx^-} jointly with x^+_t and x^-_t. Therefore, we assume $\lambda_{gx^+} > 0$ and $\lambda_{mx^-} < 0$ such that positive shocks to x^+_t and x^-_t both increase the risk premiums in stocks. The state variables associated with shocks ω^{p+}_t and ω^{p-}_t in the empirical application are therefore linked to x^+_t and x^-_t by $p^+_t = \lambda_{gx^+} x^+_t$ and $p^-_t = \lambda_{mx^-} x^-_t$.

Model specification	$\Phi_F = \text{diag}(\phi_\tau, \phi_g, \phi_m, \phi_{x^+}, \phi_{x^-})$ $\Lambda_{1(2,4)} = \lambda_{gx^+} > 0$, $\Lambda_{1(3,5)} = \lambda_{mx^-} < 0$ $0 < \delta_g < 1$ and $\delta_\tau > 1$
Nominal yields loadings B_n	$B_n^i = \frac{\delta_i}{n}\frac{1-\phi_i^n}{1-\phi_i} > 0$, $i = \{\tau, g, m\}$ $B_n^{x^+} = \frac{n-1}{n}\phi_{x^+} B_{n-1}^{x^+} - \frac{n-1}{n} B_{n-1}^g \lambda_{gx^+} < 0$ $B_n^{x^-} = \frac{n-1}{n}\phi_{x^-} B_{n-1}^{x^-} - \frac{n-1}{n} B_{n-1}^m \lambda_{mx^-} > 0$
pd ratio loadings B_s	$B_s^\tau = \frac{1-\delta_\tau}{1-\kappa_1\phi_\tau} < 0$ $B_s^g = \frac{1-\delta_g}{1-\kappa_1\phi_g} > 0$ $B_s^m = -\frac{1}{1-\kappa_1\phi_m} < 0$ $B_s^{x^+} = \frac{-\kappa_1\lambda_{gx^+} B_s^g}{1-\kappa_1\phi_{x^+}} < 0$ $B_s^{x^-} = \frac{-\kappa_1\lambda_{mx^-} B_s^m}{1-\kappa_1\phi_{x^-}} < 0$
Expected excess return on nominal bond	const. $\underbrace{-(n-1)B_{n-1}^g\lambda_{gx^+}}_{(-)} x_t^+ \underbrace{-(n-1)B_{n-1}^m\lambda_{mx^-}}_{(+)} x_t^-$
Expected excess return on stock	const. $+\kappa_1(\underbrace{B_s^g\lambda_{gx^+}}_{(+)} x_t^+ + \underbrace{B_s^m\lambda_{mx^-}}_{(+)} x_t^-)$

Table IA-5. Baseline specification.

The signs of B_n's given in Table IA-5 are consistent with the sign restrictions we impose on yields. Specifically, ω_t^g, ω_t^m and $\omega_t^{x^-}$ have a positive impact while $\omega_t^{x^+}$ has a negative impact on yields at all maturities. The monotonicity restrictions also hold in this baseline specification. B_n^g and B_n^m are monotonically decreasing with maturity n since $0 < \phi_i < 1$, $i = g, m$. The evolution of $B_n^{x^+}$ and $B_n^{x^-}$ loadings across maturities is more complex, but as long as their respective dynamics (ϕ coefficients) are sufficiently persistent, the loadings increase over the range of maturities relevant for our identification (see Appendix C.1 for more details). The signs of B_s are consistent with the restrictions we impose on stock returns: with a positive response of stock returns and the *pd* ratio to ω_t^g but a negative response to ω_t^m, $\omega_t^{x^+}$ and $\omega_t^{x^-}$. It is worth noticing that with $\delta_\tau > 1$ (Taylor principle, i.e., the short rate responding more than one-for-one to expected inflation) expected inflation shocks generate the same set of sign restrictions as monetary shocks. We return to this fact in our subsequent discussion.

F.3. Counter-cyclical inflation

The baseline case in Table IA-5 assumes no feedbacks between the state variables. We next consider the case of countercylical inflation in which higher expected inflation predicts lower expected growth. Piazzesi and Schneider (2006) and Bansal and Shaliastovich (2013) provide evidence consistent with this channel based on different specification of VAR models estimated over long samples going back to 1960s and 1970s. Replicating the VAR evidence using survey forecasts over our main sample (1983–2017), we do not find a significant negative effect of expected inflation on expected growth (see Table IA-7, Panel A). It is nevertheless useful to consider how such a channel could affect our identification.

The only change from the baseline case is that we allow $\Phi_{F(2,1)} = \phi_{g\tau} < 0$. Table IA-6 shows how this assumption affects the coefficients relative to the baseline case above.

Model specification	$diag(\Phi_F) = (\phi_\tau, \phi_g, \phi_m, \phi_{x^+}, \phi_{x^-})$ and $\Phi_{F(2,1)} = \phi_{g\tau} < 0$
Nominal yields loadings B_n	$B_n^\tau = \frac{n-1}{n}\phi_\tau B_{n-1}^\tau + \frac{n-1}{n}\phi_{g\tau} B_{n-1}^g + \frac{\delta_\tau}{n} > 0$ if small $\lvert\phi_{g\tau}\rvert$
pd ratio loadings B_s	$B_s^\tau = \frac{1+\kappa_1\phi_{g\tau}B_s^g - \delta_\tau}{1-\kappa_1\phi_\tau} < 0$

Table IA-6. Counter-cyclical inflation specification. We only report coefficients that are different from the baseline specification in Table IA-5.

The negative feedback from expected inflation to expected growth ($\phi_{g\tau}$) strengthens the negative effect of expected inflation τ_t on stocks (B_s^τ). With this modification, the sign of the loading on yields B_n^τ could, in principle, turn negative. However, there is pervasive evidence in the literature that expected inflation affects yields positively (see also Table IA-1), implying $B_n^\tau > 0$. This fact is consistent with $|\phi_{g\tau}|$ being small.[10] Indeed, Table IA-7 Panel A suggests that such a feedback effect is not statistically significantly different from zero in the post-1983 sample. As long as the signs of the loadings B_n and B_s are unchanged, the signs of the impacts of structural shocks on the risk premia remain the same as in the baseline specification.

A. Dependent variable: Real GDP growth forecast $F_t(\Delta\text{RGDP}_h)$					
	$h = 0q$	$h = 1q$	$h = 2q$	$h = 3q$	$h = 4q$
$F_{t-1}(\Delta\text{CPI}_h)$	-0.022	-0.026	-0.018	-0.013	-0.012
	(-0.74)	(-1.18)	(-1.20)	(-1.34)	(-1.22)
$F_{t-1}(\Delta\text{RGDP}_h)$	0.91***	0.92***	0.93***	0.95***	0.95***
	(21.70)	(26.25)	(37.88)	(64.00)	(50.78)
Constant	0.29*	0.27**	0.24***	0.19***	0.16**
	(1.86)	(2.28)	(2.85)	(3.46)	(2.33)
R^2	0.81	0.85	0.88	0.92	0.92
N	418	418	418	418	418
B. Dependent variable: CPI inflation forecast $F_t(\Delta\text{CPI}_h)$					
	$h = 0q$	$h = 1q$	$h = 2q$	$h = 3q$	$h = 4q$
$F_{t-1}(\Delta\text{CPI}_h)$	0.83***	0.96***	0.98***	0.99***	0.99***
	(19.09)	(62.27)	(113.31)	(137.69)	(137.76)
$F_{t-1}(\Delta\text{RGDP}_h)$	0.034	0.021	0.019*	0.014	0.018*
	(0.73)	(0.88)	(1.75)	(1.46)	(1.78)
Constant	0.37**	0.049	-0.0095	-0.012	-0.029
	(2.33)	(0.63)	(-0.24)	(-0.31)	(-0.73)
R^2	0.71	0.94	0.98	0.99	0.99
N	418	418	418	418	418

Table IA-7. Feedbacks between inflation and real GDP forecasts. The table presents VAR(1) estimates for expected CPI inflation and expected real GDP growth forecasts at different forecast horizons (between the current quarter out to four quarters ahead). The forecasts are from the BCEI survey, expressed as annualized percent change from the previous quarter. The sample period is 1983–2017. The data is sampled monthly. HAC standard errors with 3 lags are reported in parentheses.

F.4. Other channels

Finally, we consider a more comprehensive specification, which captures several important features of the post-1983 sample period. We discuss conditions under our identification restrictions continue to hold and argue that these conditions are satisfied during our sample period.

First, we set $\Phi_{F(1,2)} = \phi_{\tau g} > 0$ to capture the effect that higher expected growth can lead to higher expected inflation as when the economy is driven by demand shocks. This setting generates procyclical inflation which has characterized a large part of our sample period as argued by Campbell et al. (2017) and Campbell et al. (2020) (see also Table IA-7 Panel B). Second, we set $\Phi_{F(2,3)} = \phi_{gm} < 0$, which implies that

[10] Substituting the B_n^g from Table IA-5 into the B_n^τ under the counter-cyclical inflation specification, we have $B_n^\tau = \frac{n-1}{n}\phi_\tau B_{n-1}^\tau + \frac{1}{n}\phi_{g\tau}\delta_g\frac{1-\phi_g^{n-1}}{1-\phi_g} + \frac{\delta_\tau}{n}$. Since $0 < \phi_g < 1$, $\frac{1}{n}\phi_{g\tau}\delta_g\frac{1-\phi_g^{n-1}}{1-\phi_g}$ is negative and the absolute value is increasing in n. On the contrary, $\frac{\delta_\tau}{n}$ is positive and decreasing in n. Thus, there exists a $\bar{n}$ such that, $\forall n < \bar{n}$, $\frac{1}{n}\phi_{g\tau}\delta_g\frac{1-\phi_g^{n-1}}{1-\phi_g} + \frac{\delta_\tau}{n} > 0$. This implies, $B_n^\tau > 0$ at least for $n < \bar{n}$. A smaller $|\phi_{g\tau}|$ thus leads to a larger $\bar{n}$. The specification that $\delta_\tau > 1 > \delta_g$ also contributes to a larger $\bar{n}$.

a tighter monetary policy negatively affects future expected growth. Finally, to allow for a time-varying inflation risk premium, we further assume that expected inflation shocks ω^τ are priced with a market price of risk driven by the common premium factor x_t^-. This assumption implies that risk premia associated with expected inflation shocks and monetary shocks are determined by the same state variable, and is motivated by the fact that, under plausible parameters, τ_t and m_t generate the same sign restrictions on stocks and yields (see Table IA-5). One could interpret x_t^- as the time-varying market price of risk (as a reduced-form representation of either time-varying risk aversion or uncertainty) associated with discount rate shocks (m_t) or nominal shocks (τ_t). Thus, we set $\Lambda_{1(1,5)} = \lambda_{\tau x^-} < 0$, analogous to the market prices of risk associated with monetary shocks λ_{mx^+}.

Table IA-8 summarizes how the above assumptions alter the loadings compared to the baseline specification. Most restrictions continue to hold regardless of parameter values. When the feedback effects $|\phi_{\tau g}|$ and $|\phi_{gm}|$ are small relative to the persistence of the respective state variables (τ_t and g_t), the signs and the monotonicity of loadings remain the same as in the baseline model.[11]

Implications for nominal-real yield spread. In Appendix E, we study the empirical relationship between the nominal-real yield spread (i.e., the breakeven inflation rate) and ω shocks. It is therefore useful to analyze within the model the impact of ω shocks on the spread. The model counterpart of breakeven inflation (BEI) is the spread between the nominal yield (equation IA.55) and real yield (equation IA.59):

$$b_t^{(n)} = y_t^{(n)} - y_t^{(n),r} = \text{const.} + (B_n - B_n^r)' F_t = \text{const.} + \beta_n' F_t. \tag{IA.69}$$

The loadings β_n are reported in Table IA-8. To analyze the spread at different maturities n, we can start with the initial value and trace out the loadings recursively. When $n = 1$, we have $\beta_1^\tau = 1$, $\beta_1^g = \beta_1^m = \beta_1^{x^+} = \beta_1^{x^-} = 0$. BEI loads positively on expected inflation, $\beta_n^\tau > 0$ for all n and on expected growth $\beta_n^g > 0$, but negatively on monetary news $\beta_n^m < 0$.[12] Expected growth predicts higher expected inflation since $\phi_{\tau g} > 0$ and thus growth news affects BEI positively. A positive monetary policy shock (tightening) reduces expected growth because $\phi_{gm} < 0$ and consequently lowers expected inflation as well as BEI, since $\phi_{\tau g} > 0$.

BEI is also affected by the two risk premium factors. We have $\beta_n^{x^+} < 0$ for all $n \geq 2$, thus hedging premium shocks lower BEI. This is because with procyclical inflation ($\phi_{\tau g} > 0$) nominal bonds are a better hedge of growth risk relative to real bonds. The sign of the loading on the common premium $\beta_n^{x^-}$ is indeterminate because $\beta_n^\tau > 0$ but $\beta_n^m < 0$. However, under the assumption that the feedback effects ($|\phi_{\tau g}|$ and $|\phi_{gm}|$) are small, we would expect $|\beta_n^m|$ is much smaller than $|\beta_n^\tau|$.[13] Thus, $\beta_n^{x^+} > 0$ is primarily driven by $\beta_n^\tau > 0$, for the range of maturities we focus on. This, in turn, is consistent with the notion that nominal bonds earn a higher inflation risk premium than real bonds.

[11] Table IA-7 Panel B shows that the effect of expected growth on expected inflation (proxy for $\phi_{\tau g}$) is indeed positive, weakly significant, and economically small, relative to the persistence of expected inflation itself. Likewise, existing evidence also suggests that the feedback from monetary shocks onto growth expectations (proxy for ϕ_{gm}) is unlikely to overturn our sign restrictions. Using several different survey measures, Bauer and Swanson (2020) find that the effect of monetary policy surprises on expectations of real macro variables is negative but statistically insignificant in most specifications. They support these findings with a survey they conduct among professional economists. Our evidence in Figure 7 Panel A of the paper (coefficients $\gamma_1^{h,m}, h > 0$) is also consistent with a negative feedback of monetary shocks on growth expectations; however, the economic magnitude of the effect is small.

[12] Because $\phi_{\tau g} > 0$ and $\phi_{gm} < 0$, we have $\beta_n^g > 0$ for all $n \geq 2$ and $\beta_n^m < 0$ for all $n \geq 3$. Given the recursive structure, initially, only $\beta_1^\tau \neq 0$. In the second period, $\beta_2^g \neq 0$ through the $\phi_{\tau g}\beta_1^\tau$. Next, in the third period, $\beta_3^m \neq 0$ through the effect of $\phi_{gm}\beta_2^g$.

[13] For an intuitive illustration, we further assume $\phi_\tau = \phi_g = \phi_m$. Then, the difference between β^τ, β^g, and β^m stems only from terms 1, $(n-1)\phi_{\tau g}\beta_{n-1}^\tau$, and $(n-1)\phi_{gm}\beta_{n-1}^g$, respectively (see Table IA-8). Solving recursion for β_n^τ, we have $\beta_n^\tau = \frac{1}{n}\frac{1-\phi_\tau^n}{1-\phi_\tau}$ which is decreasing in n and $\beta_1^\tau = 1$. Thus, when $|\phi_{\tau g}|$ is small, $(n-1)\phi_{\tau g}\beta_{n-1}^\tau < 1$ for $n < \bar{n}$. This implies $|\beta_n^g| < |\beta_n^\tau| \leq 1$ for the range of maturities we use in the empirical analysis, $n < \bar{n}$. Similarly, when $|\phi_{gm}|$ is small, for $n < \bar{n}$, $|(n-1)\phi_{gm}\beta_{n-1}^g| < 1$ implies $|\beta_n^m| < |\beta_n^\tau|$.

In conclusion, BEI should load positively on growth expectations g and the common premium x^- and negatively on monetary shocks m and the hedging premium x^+. We analyze these predictions empirically in Appendix E.2.2.

Model specification	$diag(\Phi_F)$ =(ϕ_τ,ϕ_g,ϕ_m,ϕ_{x^+},ϕ_{x^-}), $\Phi_{F(1,2)} = \phi_{\tau g} > 0$ and $\Phi_{F(2,3)} = \phi_{gm} < 0$ $\Lambda_{1(2,4)} = \lambda_{gx^+} > 0$, $\Lambda_{1(3,5)} = \lambda_{mx^-} < 0$ and $\Lambda_{1(1,5)} = \lambda_{\tau x^-} < 0$
Nominal yields loadings B_n	$B_n^g = \frac{n-1}{n}\phi_g B_{n-1}^g + \frac{n-1}{n}\phi_{\tau g} B_{n-1}^\tau + \frac{1}{n}\delta_g > 0$ $B_n^m = \frac{n-1}{n}\phi_m B_{n-1}^m + \frac{n-1}{n}\phi_{gm} B_{n-1}^g + \frac{1}{n} > 0$ if small $\lvert\phi_{gm}\rvert$ $B_n^{x^-} = \frac{n-1}{n}\phi_{x^-} B_{n-1}^{x^-} - \frac{n-1}{n} B_{n-1}^\tau \lambda_{\tau x^-} - \frac{n-1}{n} B_{n-1}^m \lambda_{mx^-} > 0$
pd ratio loadings B_s	$B_s^g = \frac{1+\kappa_1\phi_{\tau g} B_s^\tau - \delta_g}{1-\kappa_1\phi_g} > 0$ if small $\lvert\phi_{\tau g}\rvert$ $B_s^m = \frac{\kappa_1\phi_{gm} B_s^g - 1}{1-\kappa_1\phi_m} < 0$ $B_s^{x^-} = \frac{-\kappa_1(\lambda_{\tau x^-} B_s^\tau + \lambda_{mx^-} B_s^m)}{1-\kappa_1\phi_{x^-}} < 0$
Expected excess return on nominal bond	const.$\underbrace{-(n-1)B_{n-1}^g\lambda_{gx^+}}_{(-)} x_t^+ \underbrace{-(n-1)(B_{n-1}^\tau\lambda_{\tau x^-} + B_{n-1}^m\lambda_{mx^-})}_{(+)} x_t^-$
Expected excess return on stock	const.$+\kappa_1(\underbrace{B_s^g\lambda_{gx^+}}_{(+)} x_t^+ + \underbrace{(B_s^\tau\lambda_{\tau x^-} + B_s^m\lambda_{mx^-})}_{(+)} x_t^-)$
Nominal-real yield spread loadings β_n	$\beta_n^\tau = \frac{n-1}{n}\phi_\tau\beta_{n-1}^\tau + \frac{1}{n} > 0$ $\beta_n^g = \frac{n-1}{n}\phi_g\beta_{n-1}^g + \frac{n-1}{n}\phi_{\tau g}\beta_{n-1}^\tau > 0$ $\beta_n^m = \frac{n-1}{n}\phi_m\beta_{n-1}^m + \frac{n-1}{n}\phi_{gm}\beta_{n-1}^g < 0$ $\beta_n^{x^+} = \frac{n-1}{n}\phi_{x^+}\beta_{n-1}^{x^+} - \frac{n-1}{n}\lambda_{gx^+}\beta_{n-1}^g < 0$ $\beta_n^{x^-} = \frac{n-1}{n}\phi_{x^-}\beta_{n-1}^{x^-} - \frac{n-1}{n}\lambda_{\tau x^-}\beta_{n-1}^\tau - \frac{n-1}{n}\lambda_{mx^-}\beta_{n-1}^m > 0$ if $\lvert\phi_{gm}\rvert$ and $\lvert\phi_{\tau g}\rvert$ are small

Table IA-8. Feedbacks between variables (procyclical inflation case). We only report coefficients that are different from the baseline specification in Table IA-5.

G. Bootstrap

Inference in set-identified structural VAR models is complex, especially from a frequentist perspective. As in our setting, there are two sources of uncertainty stemming from the estimation of the reduced-form VAR parameters and from the model multiplicity induced by the set-identified structural parameters. Faust et al. (2004) (FSW) use bootstrap-based inference and Bonferroni inequality to combine two uncertainties into one confidence interval for functions of parameters (e.g., impulse response functions and variance decompositions). Granziera et al. (2018) (GMS) provide a more general inference methodology that shares the intuition with FSW. The idea is to first generate a confidence set for structural parameters, which are derived from the estimates of the reduced-form parameters and of their asymptotic covariance matrix. Then, conditional on any single draw of structural parameters from this confidence set, one obtains bootstrap confidence set for point-identified reduced-form parameters and thus point-identified functions of interest. Finally, Bonferroni inequality is used to combine these two sets into one confidence interval. However, these methodologies only apply to inference on functions of parameters but not functions of both parameters and data. We are interested in assessing the uncertainty about the time series of structural shocks, impulse response function based on local projections (Jordà, 2005), and historical decomposition of observables.

Inspired by the literature above, we adopt a bootstrap-based approch that can jointly measure the two uncertainties and applies to functions of both parameters and data. We start by bootstrapping the reduced-form VAR model to asses the uncertainty stemming from the estimation of reduced-form parameters. As in a standard residual-based bootstrap, using the maximum-likelihood estimates of the VAR, we obtain the reduced-form shock series (residuals) and draw randomly with replacement to form an artificial shock series with the same length as the original one. We then construct an artificial yield changes and stock returns by iterating the estimated VAR model date by date with the artificial shocks and initial values equal to the data. In the next step, we apply our identification procedure on the artificial data to generate

a set of valid structural models[14] $\{\boldsymbol{\Phi}(L), \tilde{\boldsymbol{A}}\} = \{\Phi_i(L), \tilde{A}_{i,j}, j = 1, 2, ..., N_{valid}\}$ for the bootstrap trial i, where $N_{valid} = 1000$ is the number of models satisfying identification restrictions retained within each trial. By repeating the bootstrap process $N_{bs} = 1000$ times, we obtain a pool of $N_{bs} \times N_{valid}$ models $\{\Phi_i(L), \tilde{A}_{i,j}, j = 1, 2, ..., N_{valid}\}_{i=1,2,...,N_{bs}}$. The set of all structural parameters A within this pool is analogous to the set of structural parameters derived in FSW and GMS. The difference is that they draw from the analytical asymptotic distribution of reduced-form parameters, while we bootstrap the residuals.

With the $N_{bs} \times N_{valid}$ pool of models, using parameters $\{\boldsymbol{\Phi}(L), \tilde{\boldsymbol{A}}\}$, we can compute variance ratios and assess their uncertainty. However, since models are based on bootstrapped artificial data, we cannot obtain meaningful shock series and historical decompositions of asset returns over time. Therefore, for inference on objects relying on both parameters and data (e.g., structural shocks, historical decompositions, etc.), we adopt a modified bootstrap procedure. Instead of set-identifying structural parameters based on artificial reduced-form shocks, we take the VAR parameters $\Phi_i(L)$ from the bootstrap back to the original data series and reconstruct the reduced-form shocks. We then apply the identification procedure on the new reduced-form shocks and obtain $\{\tilde{A}_{i,j}\}_{j=1,2,...,N_{valid}}$. We can now back out the time series of cumulative shocks as $\{W_t^{i,j}\}_{t=1,2,..,T}$. This process results in $N_{bs} \times N_{valid}$ structural shocks series, whose distribution represents the sum of two types of uncertainty.

To illustrate estimation uncertainty alone, Figure IA-4 presents the percentiles of the median cumulative shocks ($W_t^{i,med} = \text{median}(W_t^{i,j})$) across i at each t. That is, within each bootstrap trial i, we take the median of shocks over all N_{valid} models;[15] we then construct confidence intervals as percentiles over the N_{bs} median cumulative shock series at each t. The error bands only represent the estimation uncertainty because the median of shocks in each bootstrap trial is a point estimate and therefore does not reflect model uncertainty stemming from the set identification. The narrow error bands shown in Figure IA-4 reflect the fact that the estimation uncertainty stems primarily from the estimation of the covariance matrix of the reduced-form shocks. Because yield changes and stock returns mean-revert quickly, the estimation precision of the feedback parameters in the VAR does not significantly affect the estimation of the reduced-form shocks.

[14] A structural model is defined as $\{\Phi, A\}$, a pair of reduced-form parameters and structural parameters.

[15] As argued above, the total uncertainty is represented by the distribution of all $N_{bs} \times N_{valid}$ structural shocks series. We can view this distribution as a joint distribution $f(\Phi, A)$ of both reduced-form and structural parameters, where $f(\cdot, \cdot)$ represents the pdf. Then, to eliminate model uncertainty, we should integrate over structural parameters. We use the median of shocks rather than shocks from the MT solution because taking median of shocks over structural parameters better represents this integral operation (MT solution is a non-linear operator over the distribution).

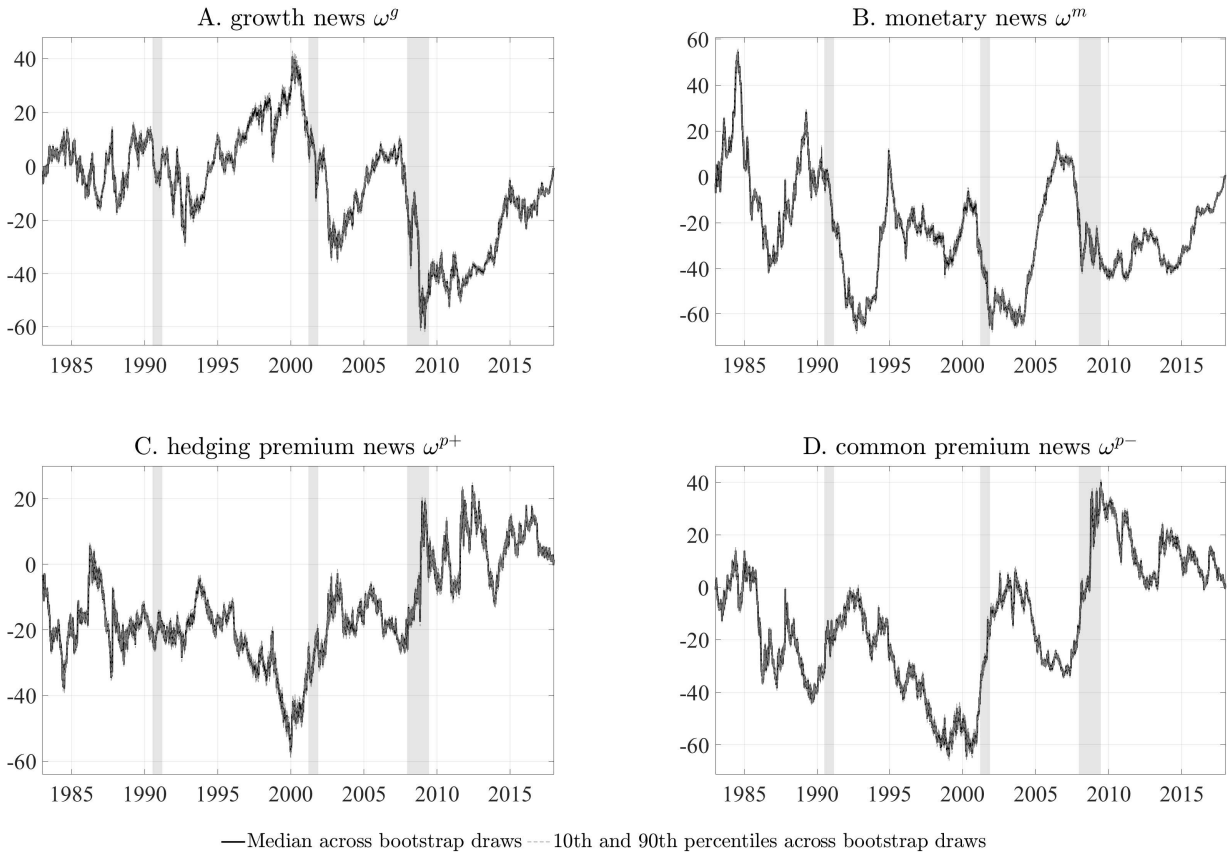

Figure IA-4. Estimation uncertainty. The figure presents the median, the 10th, and the 90th percentiles of the bootstrap distribution of the median of cumulative shocks. The bootstrap procedure is explained in Appendix G.

H. Additional tables and figures

Study	Effect on stocks	Effect on yields	Main sample period
Monetary shocks (tightening news)			
Poole et al. (2002)	n/a	+, ↘	pre-1994, 1994-2002
Rigobon and Sack (2004)	−	+, ↘	1994:1-2001:11
Gürkaynak et al. (2005b)	n/a	+, ↘	1990:1-2002:12
Bernanke and Kuttner (2005)	−	+, ↘	1989:6-2002:12
Gürkaynak et al. (2005a)	−	+, ↘	1990:1-2004:12
Campbell et al. (2012)	n/a	+, ↘	1990:2-2007:6, 2007:8-2011:12
Hanson and Stein (2015)	n/a	+, ↘	1999:1-2012:2
Nakamura and Steinsson (2018)	−	+, ↘	1995-2014

Table IA-9. Literature on identification of monetary shocks and their effect on stocks and the yield curve. The table summarizes the evidence on the effect of monetary policy shocks on stocks and yields. + (−) describes the direction of the effect, ↘ indicates that the effect declines across the term structure.

	(1)	(2)	(3)	(4)
	$\lvert\omega^g\rvert$	$\lvert\omega^m\rvert$	$\lvert\omega^{p+}\rvert$	$\lvert\omega^{p-}\rvert$
FOMC day dummy	0.057	0.27***	-0.033	0.049
	(0.85)	(3.33)	(-0.73)	(0.82)
Constant	0.71***	0.75***	0.69***	0.67***
	(58.61)	(60.79)	(60.90)	(64.58)
N (days)	3784	3784	3784	3784

Table IA-10. FOMC dummy regressions. The table reports regressions of absolute values of identified shocks on the FOMC announcement day dummy for scheduled FOMC announcements. Shocks are expressed in units of standard deviations. Regressions are estimated over the 1994–2008 sample, covering 120 scheduled FOMC meetings. t-statistics robust to heteroscedasticity are reported in parentheses.
We consider only scheduled FOMC meetings over the 1994–2008 sample to focus on days that are less likely to be contaminated by other types of news. Unscheduled FOMC announcements are usually interpreted as the Fed's response to other (unexpected) news events (e.g., Bernanke and Kuttner, 2005), and thus may not reflect monetary news. We also omit the post-2008 period, when the Fed launched an array of unconventional policy measures that affected asset prices through multiple channels, as we show in Section 4.4. The use of absolute values (as opposed to signed shocks) serves to quantify the *amount* of news that comes out on FOMC days relative to other days, not the *direction* of news. The only significant slope coefficient is for monetary shocks (column (2)). The absolute magnitude of ω^m shocks is 36% higher (= 0.27/0.75) on FOMC days compared to other days and the difference is strongly significant (p-value of 0.1%). The volatility of other shocks is not significantly different on FOMC days from other days. This result makes sense given that days other than FOMC days also contain large announcements that can move risk premia and growth expectations in a significant way. Similarly, because a non-negligible portion of the Fed's communication happens outside of regularly scheduled FOMC meetings (and thus affects the regression intercept), the coefficient in column (2) is a conservative measure of the amount of monetary news on FOMC days.

A. Monthly frequency ($N = 420$)

Variables	ω^g	ω^m	ω^{p+}	ω^{p-}
ω^g	1.00			
ω^m	0.13	1.00		
	(0.01)			
ω^{p+}	0.03	-0.14	1.00	
	(0.57)	(0.00)		
ω^{p-}	-0.03	-0.07	-0.07	1.00
	(0.49)	(0.14)	(0.15)	

B. Quarterly frequency ($N = 139$)

Variables	ω^g	ω^m	ω^{p+}	ω^{p-}
ω^g	1.00			
ω^m	0.25	1.00		
	(0.00)			
ω^{p+}	-0.23	-0.17	1.00	
	(0.01)	(0.05)		
ω^{p-}	-0.10	-0.24	-0.05	1.00
	(0.26)	(0.00)	(0.53)	

Table IA-11. Correlations of aggregated model-based shocks. The table displays correlations of monthly and quarterly sums of daily shocks from the model. The model is estimated at the daily frequency over the 1983–2017 sample. Daily shocks are uncorrelated by construction. Correlation p-values are in parentheses.

A. Monthly frequency

Variables	$\widehat{cf}$	CP	KP	EP 0-1m	EP 1-2m	EP 2-3m	EP 4-6m	EP 7-12m
$\widehat{cf}$	1.00							
CP	0.69	1.00						
	(0.00)							
	419							
KP	0.02	-0.05	1.00					
	(0.76)	(0.41)						
	335	335						
EP 0-1m	-0.12	0.05	0.17	1.00				
	(0.10)	(0.53)	(0.02)					
	190	190	177					
EP 1-2m	-0.18	-0.00	0.18	0.91	1.00			
	(0.01)	(0.95)	(0.02)	(0.00)				
	190	190	177	190				
EP 2-3m	-0.25	-0.07	0.11	0.56	0.78	1.00		
	(0.00)	(0.33)	(0.16)	(0.00)	(0.00)			
	192	192	179	190	190			
EP 4-6m	-0.20	-0.03	0.11	0.75	0.84	0.79	1.00	
	(0.01)	(0.64)	(0.14)	(0.00)	(0.00)	(0.00)		
	192	192	179	190	190	192		
EP 7-12m	-0.09	0.05	0.08	0.57	0.62	0.50	0.59	1.00
	(0.23)	(0.48)	(0.27)	(0.00)	(0.00)	(0.00)	(0.00)	
	192	192	179	190	190	192	192	

B. Quarterly frequency

Variables	$\widehat{cf}$	CP	KP	EP 0-1m	EP 1-2m	EP 2-3m	EP 4-6m	EP 7-12m	CAY
CAY	-0.01	-0.07	0.14	0.53	0.51	0.48	0.47	0.38	1.00
	(0.89)	(0.43)	(0.14)	(0.00)	(0.00)	(0.00)	(0.00)	(0.00)	
	138	138	112	63	63	63	63	63	

Table IA-12. Correlations of innovations to measures of bond and equity risk premium. The table presents correlations of innovations to alternative measures of bond and equity risk premium from Cieslak and Povala (2015, $\widehat{cf}$) , Cochrane and Piazzesi (2005, CP), Kelly and Pruitt (2013, KP), Martin (2017, EP), and Lettau and Ludvigson (2001, CAY). The innovations are obtained as residuals from an AR(p) process, with the number of lags selected using BIC. The p-values are included in parentheses. For each pair of variables, we also report the number of observations involved in the calculation. Since CAY is available at the quarterly frequency, its correlations with all other variables are reported separately in Panel B. Expect for forward equity premia (EP), the sample starts in 1983. The end of the sample depends on the data availability as reported in Table 3 in the main text.

	$0 \to 12m$	$0 \to 1m$	$1 \to 2m$	$2 \to 3m$	$4 \to 6m$	$7 \to 12m$
ω^g	-0.348***	-0.338***	-0.297***	-0.167***	-0.241***	-0.193***
	(-19.59)	(-16.85)	(-16.08)	(-9.52)	(-12.53)	(-8.77)
ω^m	0.277***	0.261***	0.243***	0.133***	0.191***	0.156***
	(18.07)	(12.14)	(13.98)	(7.90)	(11.52)	(8.74)
ω^{p-}	0.248***	0.290***	0.242***	0.100***	0.188***	0.099***
	(14.55)	(11.06)	(12.58)	(6.99)	(11.00)	(4.15)
ω^{p+}	0.416***	0.422***	0.382***	0.222***	0.300***	0.194***
	(23.14)	(17.35)	(17.60)	(11.80)	(16.32)	(10.90)
R^2	0.56	0.57	0.45	0.14	0.28	0.14
$R^2(\omega^{p-}, \omega^{p+})$	0.38	0.40	0.32	0.094	0.20	0.083
N (days)	4051	4051	4051	4051	4051	4051

Table IA-13. Innovations to the forward equity risk premium. The table presents regressions of daily changes in the forward equity premium bound from Martin (2017) on ω shocks. The sample period is 1996:01–2012:01.

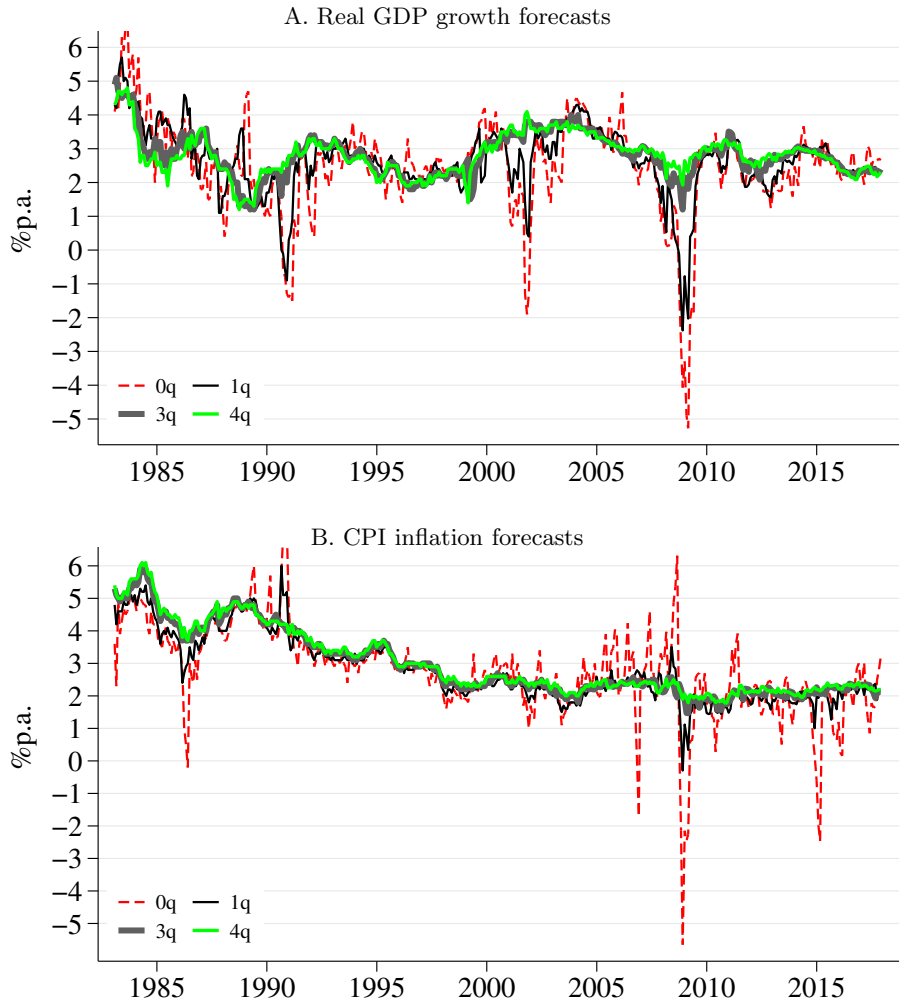

Figure IA-5. BCEI survey forecasts of real GDP growth and CPI inflation. The figure presents forecasts of real GDP growth and inflation from the BCEI survey. The forecasts are expressed as percent changes from the pervious quarter (at annual rates). Horizon h is in quarters. We plot series from the current quarter ($h = 0q$) up to ($h = 4q$) quarters ahead. For clarity of the graph, we do not display series for $h = 2q$.

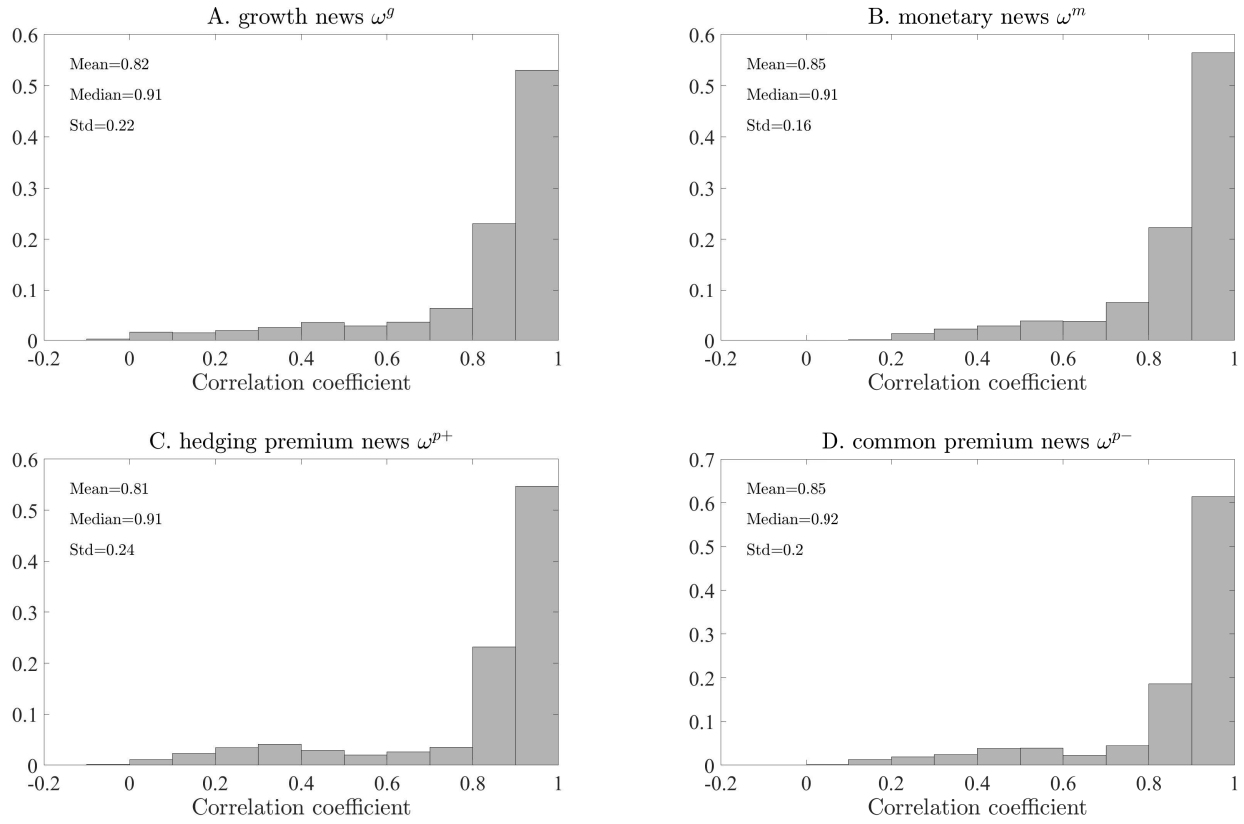

Figure IA-6. Correlation of shocks from different models. The figure presents the distribution of correlation coefficients between MT solution and other retained solutions. For each structural shock j associated with solution i we calculate its correlation with shock j associated with the MT solution, and plot the histogram of the correlation coefficients across all retained solutions. The y-axis reports the empirical probability of a correlation coefficient falling into a given bin.

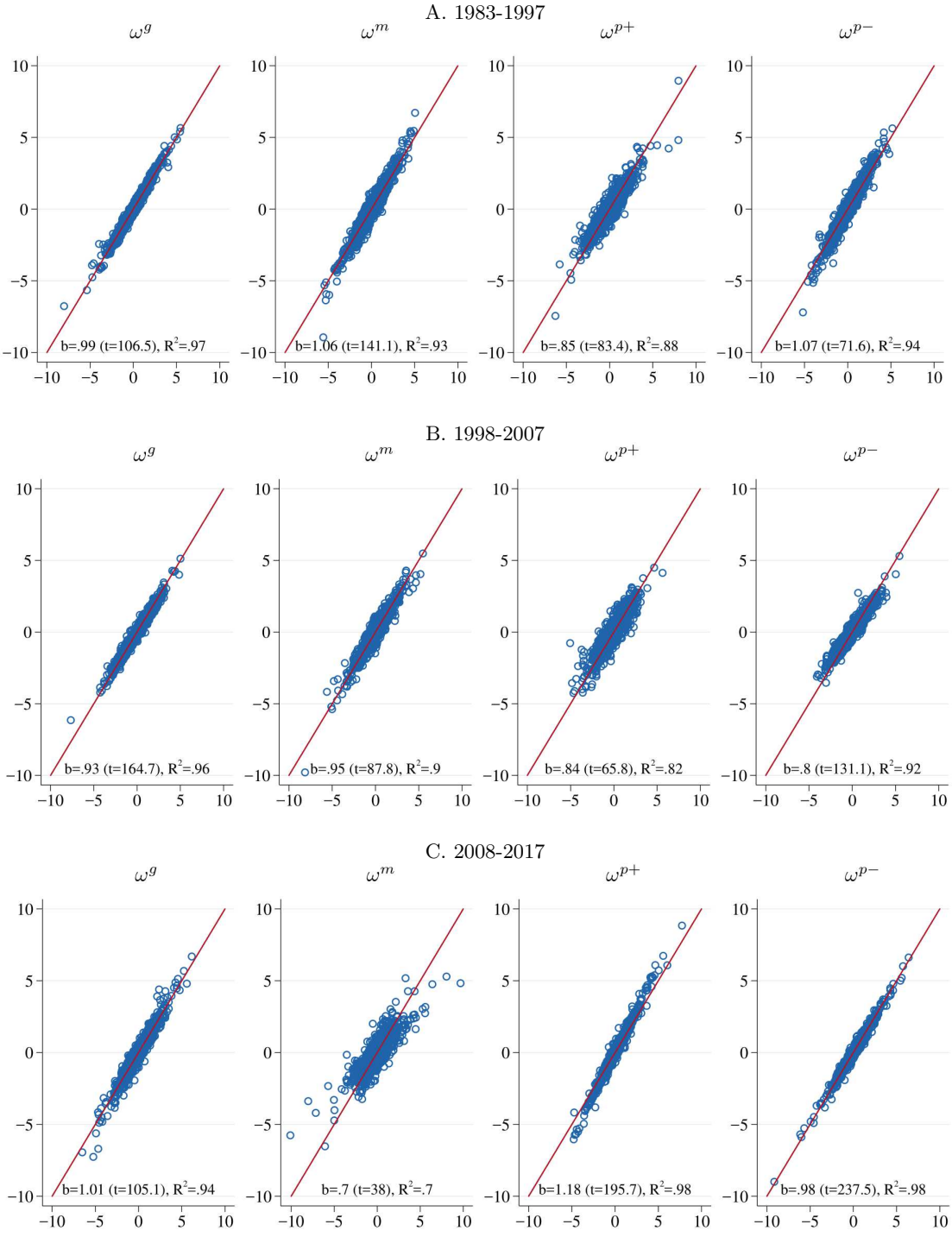

Figure IA-7. Shocks estimated over subsamples. The figure presents scatter plots of shocks estimated over the full sample, 1983–2017 (on the y-axis) against shocks estimated over subsamples (on the x-axis). Each plot contains a 45-degree line, and reports the slope coefficient, robust t-statistic and R^2 from a regression of full-sample shocks on the subsample shocks. The subsample shocks are guaranteed to have a unit standard deviation.

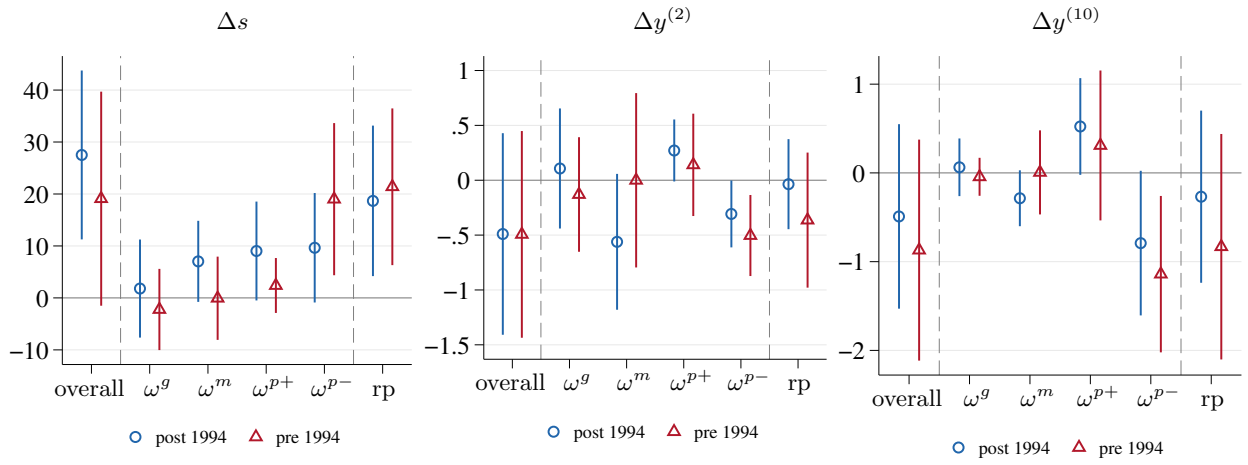

Figure IA-8. Stock returns and yield changes on FOMC days: Pre- and post-1994 comparison. The figure compares the results from regression (11) over the pre- and post-1994 samples. The post-1994 results are the same as reported in Figure 2. The pre-1994 results are based on the shocks estimated using data through the end of 1997 (when the stock-bond covariance switched sign), with results being quantitatively and qualitatively similar if we use shocks estimated over the full 1983–2017 sample. The spikes indicate 95% confidence intervals based on standard errors robust to heteroscedasticity.

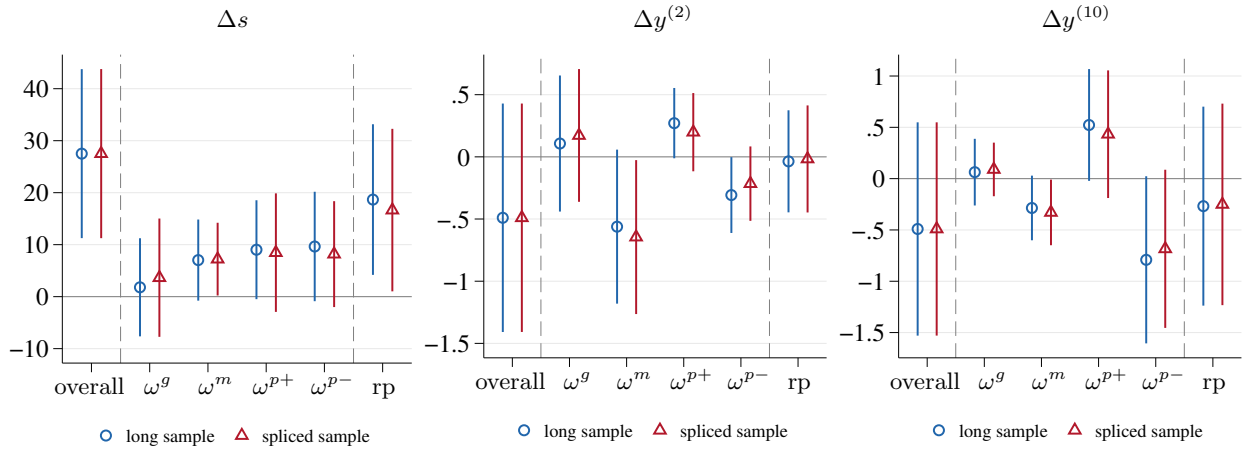

Figure IA-9. Stock returns and yield changes on FOMC days: Spliced sample estimates. The figure provides a robustness check to Figure 2, by comparing coefficients of regression (11) obtained using two sets of shocks and historical decompositions (HD) of asset returns. For the "long sample" results, shocks and HDs are estimated over the entire 1983–2017 period; for the "spliced sample" results, they are estimated separately over the 1983–1997 and 1998–2017 periods and combined. In both cases, the regressions in equation (11) are estimated over the 1994–2017 sample. The spikes indicate 95% confidence intervals based on standard errors robust to heteroscedasticity.

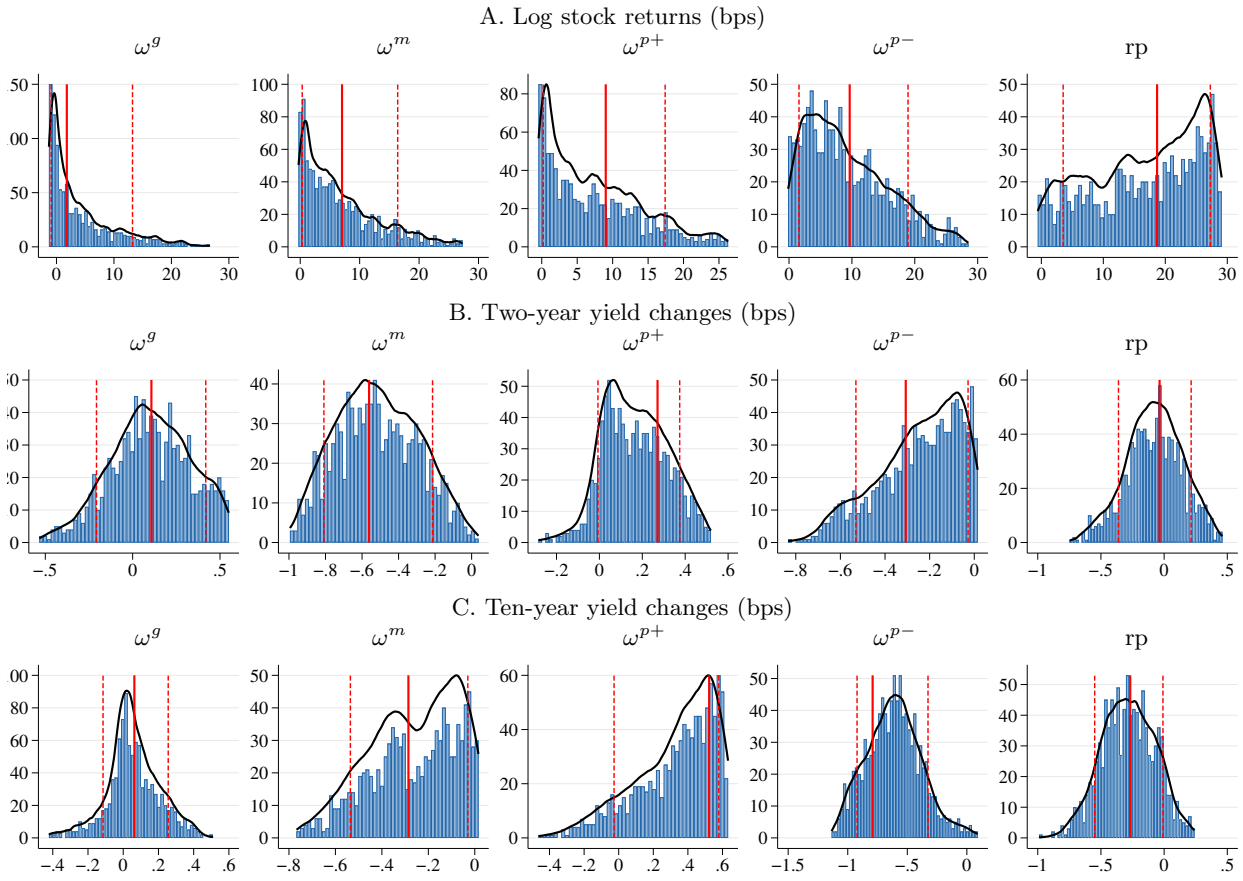

Figure IA-10. FOMC day dummy regressions across all retained solutions. The figure reports distribution of regression slope coefficients of historical decompositions of stock returns and yield changes on the FOMC day dummy for scheduled FOMC meetings (equation (11)) across all retained solutions. All coefficients are in basis points. The solid vertical line indicates the coefficients for the MT solution (corresponding to results reported in Figure 2 of the paper). The dashed vertical lines mark the 10th/90th percentiles of the distribution of slope coefficients. In each subplot, the dependent variable is the historical decomposition (10) representing the part of the overall yield change (stock return) explained by a particular shock. For example, histogram for ω^g reports slope coefficients γ_1 from the regressions $\Delta s_t(\omega_t^g) = \gamma_0 + \gamma_1 1_{t,\text{FOMC}} + \varepsilon_t$, estimated for each of the 1000 retained models. The utmost right subplot in each panel separately reports the regressions for the component due to risk premium shocks (e.g., for stocks the dependent variable is $\Delta s(\omega^{p+}) + \Delta s(\omega^{p-})$). Regressions are estimated over the 1994–2017 sample, covering 192 scheduled FOMC meetings. Shocks for all models are estimated over the 1983–2017 sample.

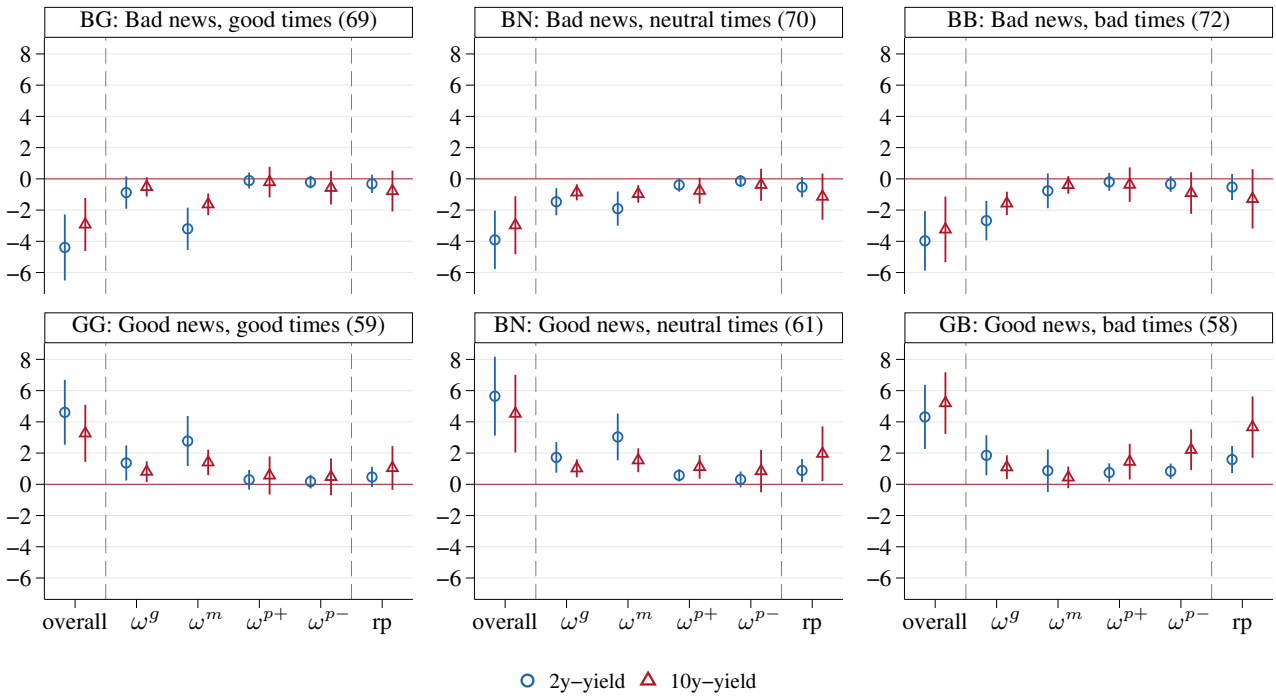

Figure IA-11. Yield changes on days of employment report announcement. The figure reports average two- and ten-year yield changes and their decompositions into contributions of structural shock on NFP announcement days, conditional on the type of news and the state of the economy. All numbers are in basis points. Good/Bad NFP news corresponds to the positive/negative NFP surprises (actual less expected NFP). The state of the economy (Good/Neutral/Bad times) is measured using the terciles of the Gap variable, Gap = −(Current unemployment − Natural rate of unemployment), with Gap in top tercile indicating good times. The estimates are obtained as β_k coefficients from regression (12), $k = \{\text{BG, BN, BB, GG, GN, GB}\}$. Each subplot combines estimates of β_k for a given k from six regressions, using a different dependent variable each. The sample period is 1985:2–2017, with 389 NFP announcements for which we have both survey and actual numbers, excluding announcements that fall on a holiday. NFP surprises before 1997 are from Money Market Services, and from 1997 onward from Bloomberg. In parentheses, we report the number of NFP announcements falling into bin k. The spikes indicate 95% confidence intervals based on robust standard errors.

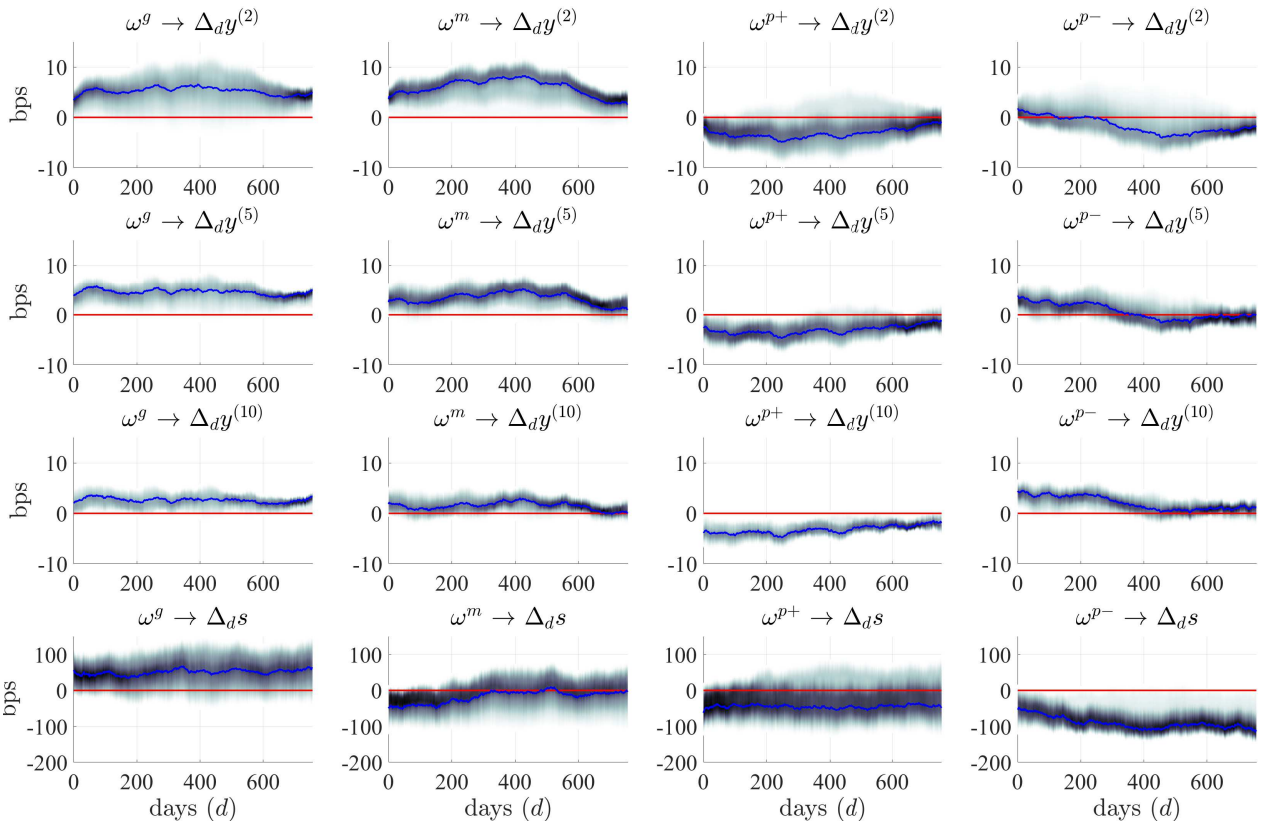

Figure IA-12. Impulse-response functions: All retained solutions, 1983–2017 sample. The figure accompanies Figure 4 in the paper. We report the distribution of responses of yield changes and stock returns to ω shocks across all 1000 retained solutions. The plots are constructed as follows: We estimate Jorda's local projections (equation (13)) for each retained solution and each horizon d. Then, for each d, we estimate a kernel density using $\beta_d^{k,j,i}$, $k = 1, ..., 1000$. We combine kernel densities across horizons d to generate a 3D surface plot where axes correspond to the horizon (x-axis), the value of β (y-axis), and the kernel density (z-axis). Finally, we generate a 2D version by viewing the 3D surface plot along the z-axis. The darker color indicates more mass of the distribution. The impulse-response function from the MT solution is displayed as the thick solid line on each subplot.

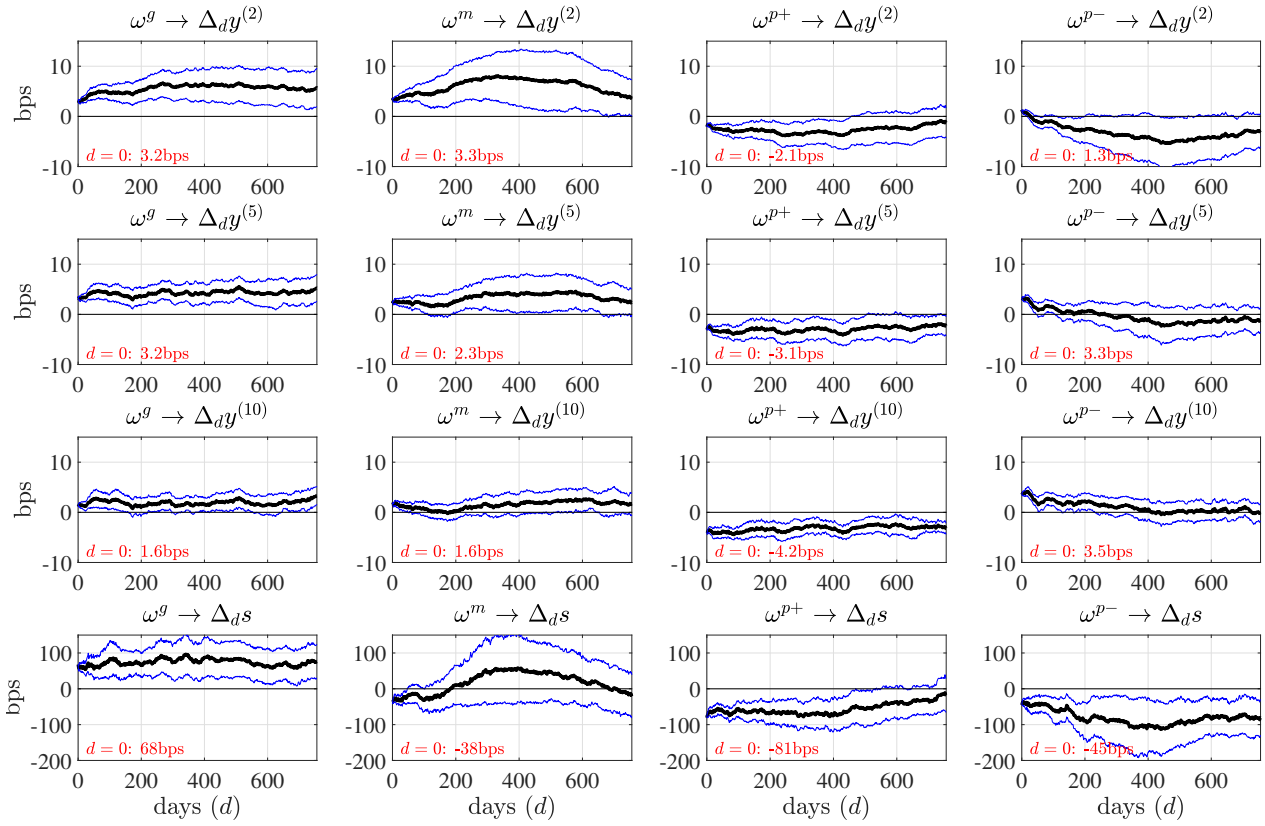

Figure IA-13. Impulse-response functions: 1998–2017 sample. The figure presents impulse-response functions of yield changes and log stock returns to ω shocks. The shocks and the impulse responses are estimated on the 1998–2017 sample for comparison with Figure 4 in the paper, which is based on the 1983–2017 sample. Shocks correspond to the MT solution and are measured in units of standard deviation. Yield changes and stock returns are in basis points. $\Delta_d x$ is a d-day change in variable x. The thick line traces out the coefficients $\beta_d^{j,i}$ from regression (13). A coefficient of 10 implies an asset response of 10 bps to a one-standard-deviation shock. The thin lines mark 95% confidence intervals calculated with Newey-West adjustment using $d+1$ lags. The numbers in the bottom left corner of each graph report the size of on impact response (for $d = 0$).